JACS
JOURNAL OF THE AMERICAN CHEMICAL SOCIETY
pubs.acs.org/JACS
Article

Targeted Solvatochromic Fluorescent Probes for Imaging Lipid Order in Organelles under Oxidative and Mechanical Stress

Dmytro I. Danylchuk, Pierre-Henri Jouard, and Andrey S. Klymchenko*

Cite This: https://dx.doi.org/10.1021/jacs.0c10972
Read Online

ABSTRACT: Biomembranes constitute a basis for all compartments of live cells, and therefore, the monitoring of their lipid organization is essential for understanding cell status and activity. However, the sensing and imaging of lipid organization specifically in different organelles of live cells remain challenging. Here, we designed an array of solvatochromic probes based on Nile Red bearing ligands for specific targeting of the endoplasmic reticulum, mitochondria, lysosomes, Golgi apparatus, plasma membranes, and lipid droplets. These polarity-sensitive probes detected variations in the lipid order by changing their emission maximum, as evidenced by fluorescence spectroscopy in model membranes. In colocalization microscopy experiments with reference organelle markers, they exhibited good organelle selectivity. Using two-color fluorescence microscopy, the new probes enabled imaging of the local polarity of organelles in live cells. To exclude the biased effect of the probe design on the sensitivity to the membrane properties, we calibrated all probes in model membranes under the microscope, which enabled the first quantitative description of the lipid order in each organelle of interest. Cholesterol extraction/enrichment confirmed the capacity of the probes to sense the lipid order, revealing that organelles poor in cholesterol are particularly affected by its enrichment. The probes also revealed that oxidative and mechanical stresses produced changes in the local polarity and lipid order that were characteristic for each organelle, with mitochondria and lysosomes being particularly stress sensitive. The new probes constitute a powerful toolbox for monitoring the response of the cells to physical and chemical stimuli at the level of membranes of individual organelles, which remains an underexplored direction in cellular research.

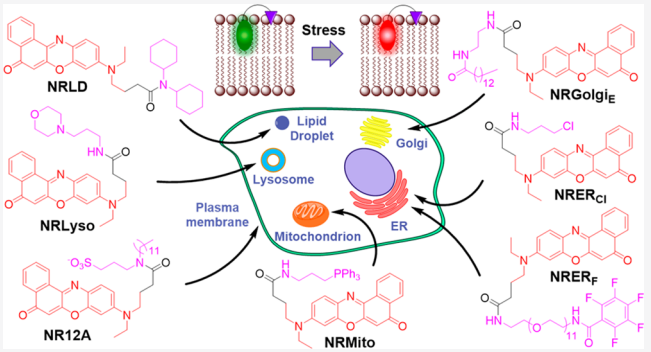

INTRODUCTION

The specific targeting and imaging of organelles in live cells have attracted significant interest in recent years.[1−8] Different strategies, utilized to achieve organelle selectivity, typically exploit biological or chemical methods by tethering fluorophores either to biomolecules, such as peptides, lipids, and oligosaccharides, or to chemically designed moieties.[1] Organelle targeting is particularly interesting to monitor the organization of lipids, which are building blocks for all live cell compartments, present either in forming membrane bilayers[9,10] or spherical core−shell structures (lipid droplets, LDs).[11] Lipid organization in biomembranes is controlled by cholesterol (Chol) and sphingomyelin (SM), which are enriched in cell plasma membrane but are less abundant in the intracellular membranes.[12,13] These lipids constitute the liquid ordered (Lo) phase,[14] which plays a crucial role in the formation of lipid microdomains.[9,10,15] The unsaturation degree of phospholipids is also of primary importance for biomembrane organization, as saturated lipids favor Lo and gel phases, while unsaturated lipids constitute the liquid disordered (Ld) phase.[10,16] Lipid unsaturation is finely tuned by the cells to preserve lipid organization,[17] and the distribution of unsaturated lipids is uneven due to enzymes, such as desaturases, present in the endoplasmic reticulum (ER).[18] On the contrary, most triglycerides and cholesterol esters are localized in LDs, a storage of energy and lipids, maintaining homeostasis of cells and protecting them from stress conditions.[19]

Environment-sensitive fluorophores such as molecular rotors, mechanosensitive, and solvatochromic dyes enable monitoring of the lipid organization of cell organelles by detecting local viscosity, mechanical tension, and polarity, respectively.[20,21] Molecular rotors, operating by the excited-state planarization of dyes with a high rotational freedom, were successfully used to monitor membrane viscosity, especially using fluorescence lifetime imaging.[20,22,23] BODIPY molecular rotor bearing a membrane anchor moiety has been proposed for imaging microviscosity in cell plasma membranes.[24]

Received: October 17, 2020

https://dx.doi.org/10.1021/jacs.0c10972
J. Am. Chem. Soc. XXXX, XXX, XXX−XXX

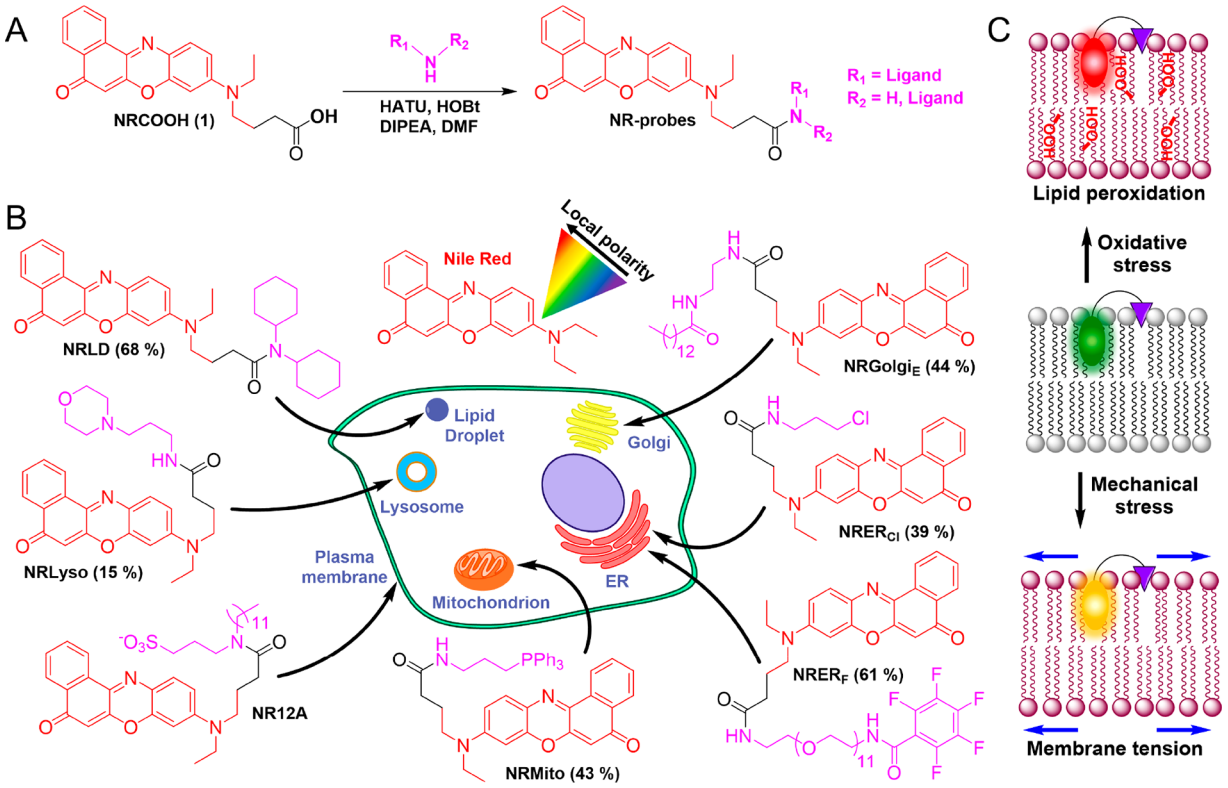

Figure 1. Organelle-targeted solvatochromic probes based on Nile Red. (A) General scheme of synthesis, and (B) chemical structures (and the reaction yields) of the developed probes (NR12A was reported previously[58]). (C) Presentation of the color response of a solvatochromic probe to oxidative and mechanical stress in lipid membranes.

Organelle-targeted molecular rotors have been also recently reported by using a genetically encoded protein tag (HaloTag), which enable sensing microviscosity in the cytosol, nucleus, ER, and mitochondria.[25] Mechanosensitive dyes based on ground-state planarization (flippers)[26,27] have emerged as powerful probes for membrane tension, a parameter that also correlates with the lipid order in biomembranes.[28,29] Their conjugates with organelle-targeting chemical groups enabled the monitoring of membrane-tension specifically in plasma membranes, mitochondria, ER, and lysosomes.[5] Their reactive derivatives (HaloFlippers) for labeling the HaloTag fused to membrane proteins have also been recently developed for probing biomembranes in any desired organelles of interest.[30]

Solvatochromic dyes, which are push−pull fluorophores undergoing excited-state charge transfer, change their emission color in response to polarity. These dyes can report on the physical state of biomembranes[31] and its alterations during apoptosis,[32,33] starvation,[34] and oxidative stress[34] while also distinguishing normal and cancerous cells.[35,36] Owing to their sensitivity to membrane hydration, dielectric properties (polarity), and solvent relaxation, solvatochromic dyes are particularly suitable for probing lipid order.[21,37,38] Indeed, in the tightly packed Lo phase, characterized by lower hydration, polarity, and fluidity, they show blue-shifted emission compared to in the Ld phase.[31] A variety of solvatochromic dyes has been applied for this purpose, including Laurdan,[39] styrylpiridinium dyes,[40,41] 3-hydroxyflavones,[42] Nile Red,[43] push−pull anthracene,[44] pyrenes,[45,46] dioxaborine,[34] etc. Previously, the efforts were mainly focused on targeting cell plasma membranes with solvatochromic dyes by grafting both charged and lipophilic groups, as exemplified for Di-4-ANEPPDHQ,[40] C-Laurdan,[47] Pro12A,[48] F2N12S,[33] NR12S,[43] etc. However, the imaging of intracellular membranes with solvatochromic dyes emerged only in recent years. Two approaches have been followed. The first one used a nonspecific lipophilic probe that redistributes in biomembranes of different organelles within the cell, thus allowing for polarity and lipid order mapping irrespectively to a given organelle.[34,45,46,49] It revealed that the intracellular biomembranes are significantly more polar (less ordered) than plasma membranes.[46] The second approach exploited the specific targeting of solvatochromic dyes to the organelle of interest,[5,25,35,36,50−53] including mitochondria[32,50,54] and ER.[35] However, these studies were focused on targeting one particular organelle. The specific targeting of different organelles using a family of probes based on the same solvatochromic dye would enable a direct comparison of the properties of organelles and their response to different stress conditions.

Nile Red, originally proposed as a lipid droplet marker,[55] has a favorable position among existing solvatochromic dyes, because it combines high brightness, operation in the optimal (yellow-red) spectral region, and good sensitivity to the lipid order.[43] Due to its fluorogenic character, it enabled spectrally resolved super-resolution (PAINT) imaging of the lipid order.[56,57] Functionalization of Nile Red with the membrane anchor groups led to a family of probes, NR12S, NR12A, and NR4A, for ratiometric and spectral imaging of the lipid order specifically in the plasma membranes.[43,58] In particular, the functionalization of Nile Red at the amino end was found to improve dye photostability, which is crucial for advanced microscopy.[58] Therefore, we considered that the functionalization of Nile Red with organelle-targeting groups could yield a

https://dx.doi.org/10.1021/jacs.0c10972
J. Am. Chem. Soc. XXXX, XXX, XXX−XXX

Table 1. Fluorescence Properties of Probes in Organic Solvents and Lipid Vesicles of Different Compositions[a]

		probe							
solvent or medium		NRMito	NRLyso	NR ER_F	NR $Golgi_E$	$NRER_{Cl}$	NRLD	NR12A[b]	Nile Red[b]
DOPC	λ_{max}em	641	640	647	630	639	645	641	639
	QY, %	43	36	34	21	38	61	51	55
DOPC/Chol	λ_{max}em	632	626	644	618	632	626	636	636
	QY, %	50	41	48	31	55	61	47	71
SM/Chol	λ_{max}em	639	587	653	586	586	582	592	589
	QY, %	24	40	21	28	56	47	39	52
phosphate buffer	λ_{max}em	660	659	654	736	653	743	648	666
	QY, %	6.9	5.8	9.5	0.4	6.5	0.33	0.36	4.2
MeOH	λ_{max}em	643	643	642	642	645	646	641	641
	QY, %	37	41	43	41	42	42	44	38
acetone	λ_{max}em	612	584	615	615	613	615	619	615
	QY, %	59	58	74	77	86	74	70	70
dioxane	λ_{max}em	602	580	591	586	584	584	602	585
	QY, %	74	53	78	78	75	78	70	74

[a]The probe concentration was 2 μM. For liposomes, the total lipid concentration was 1 mM. [b]Data from a previous work.[58]

powerful toolbox for addressing polarity and lipid order in any desired organelle in live cells.

In the present work, we synthesized a family of Nile Red derivatives bearing chemical groups for the specific targeting of organelles, such as mitochondria, ER, Golgi apparatus, lysosomes, and LDs, in addition to plasma membranes. The new probes preserved the sensitivity of Nile Red to lipid order in lipid membranes. Cellular studies confirmed their organelle-specific targeting. These probes revealed that each organelle is characterized by its unique polarity/lipid order profiles, which vary in different ways under oxidative and mechanical stress.

RESULTS AND DISCUSSION

In order to obtain solvatochromic organelle-specific probes, we conjugated a Nile Red fluorophore with targeting moieties (Figure 1A). We have already reported the plasma membrane targeting of Nile Red using alkyl sulfonate with a dodecyl chain (probe NR12A).[58] Conjugation from the amino end of Nile Red dye improved its performance compared to that using a phenolic group;[58] therefore, we selected the amino-end conjugation strategy for all organelle-targeting probes. To target mitochondria, we used triphenylphosphonium,[59] which is known to accumulate in mitochondria by crossing the inner mitochondrial membrane driven by the transmembrane potential.[1,5,60,61] *N*-Alkylmorpholin moiety, owing to its reversible protonation at a physiological pH, was used for lysosomes.[1,5,52,62] Propyl chloride[1,63] and pentafluorophenyl[5,35,60] were used for targeting ER, whereas myristic acid was used for targeting Golgi apparatus.[64] To improve the affinity of Nile Red to lipid droplets, we grafted it to two cyclohexyl moieties, which we earlier used in LDs-specific statomerocyanines.[65] All probes were synthesized starting from the previously reported[58] Nile Red derivative bearing carboxylic acid (NR-COOH). The products were obtained in moderate to good yields by an amide coupling with the corresponding targeting ligands (Figure 1, see Figure S1 of the Supporting Information).

Owing to the lipophilic nature of the Nile Red moiety, the designed probes are expected to report the local polarity and lipid order in biomembranes of specific organelles by their characteristic emission wavelengths. Moreover, they are expected to sense the cholesterol content in biomembranes of organelles, oxidative stress due to a change in polarity of biomembranes caused by lipid peroxidation,[34] and hyperosmotic shock due to an altered lipid order in organelle membranes, associated with mechanical stress (Figure 1C).[58,66]

In organic solvents of different polarities, all new probes showed high fluorescence quantum yields and solvatochromic shifts with a band position similar to that of parent Nile Red (Table 1 and Table S1), which indicates that the fluorophore preserved its optical properties, including solvatochromism. Then, we studied the probes in large unilamellar vesicles (LUVs), which are model lipid membranes of different compositions presenting Ld phase (1,2-dioleoyl-*sn*-glycero-3-phosphocholine, DOPC, and DOPC/Chol) and Lo phase (SM/Chol). In DOPC LUVs, all probes showed fluorescence enhancement with good quantum yields compared to the buffer, which was accompanied by a blue-shifted emission around 640−650 nm (Table 1, Figure 2, and Figure S2). These

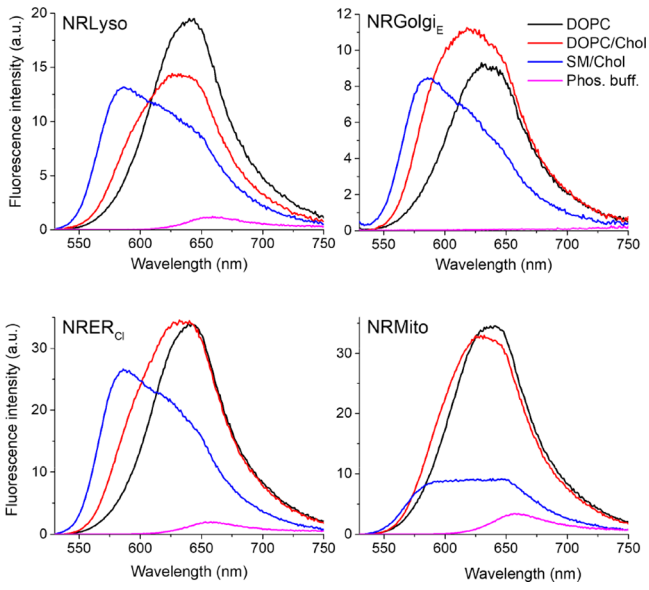

Figure 2. Fluorescence emission spectra of probes NRlyso, $NRGolgi_E$ $NRER_{Cl}$, and NRMito in lipid vesicles (LUVs) of different compositions. The probe concentration was 2 μM, the total lipid concentration was 1 mM, and the excitation wavelength was 520 nm.

https://dx.doi.org/10.1021/jacs.0c10972
J. Am. Chem. Soc. XXXX, XXX, XXX−XXX

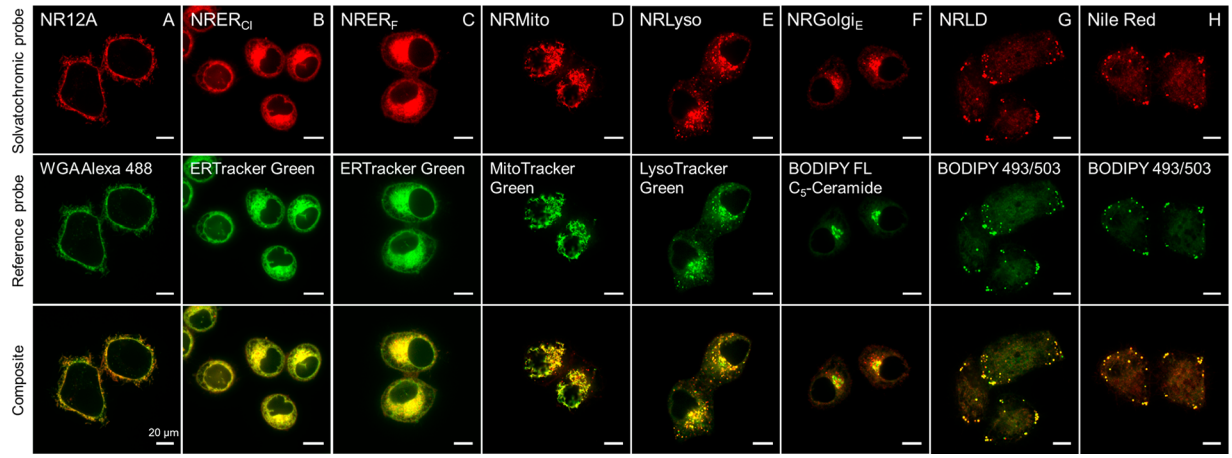

Figure 3. Colocalization of solvatochromic probes (in red) with commercial organelle probes (in green) in live KB cells. Solvatochromic probe concentrations: 20 nM for NR12A; 50 nM for NRMito, NRLyso, NRLD, and NRER$_{Cl}$; 200 nM for NRER$_F$; 2.5 μM (in form of BSA complex) for NRGolgi$_E$.

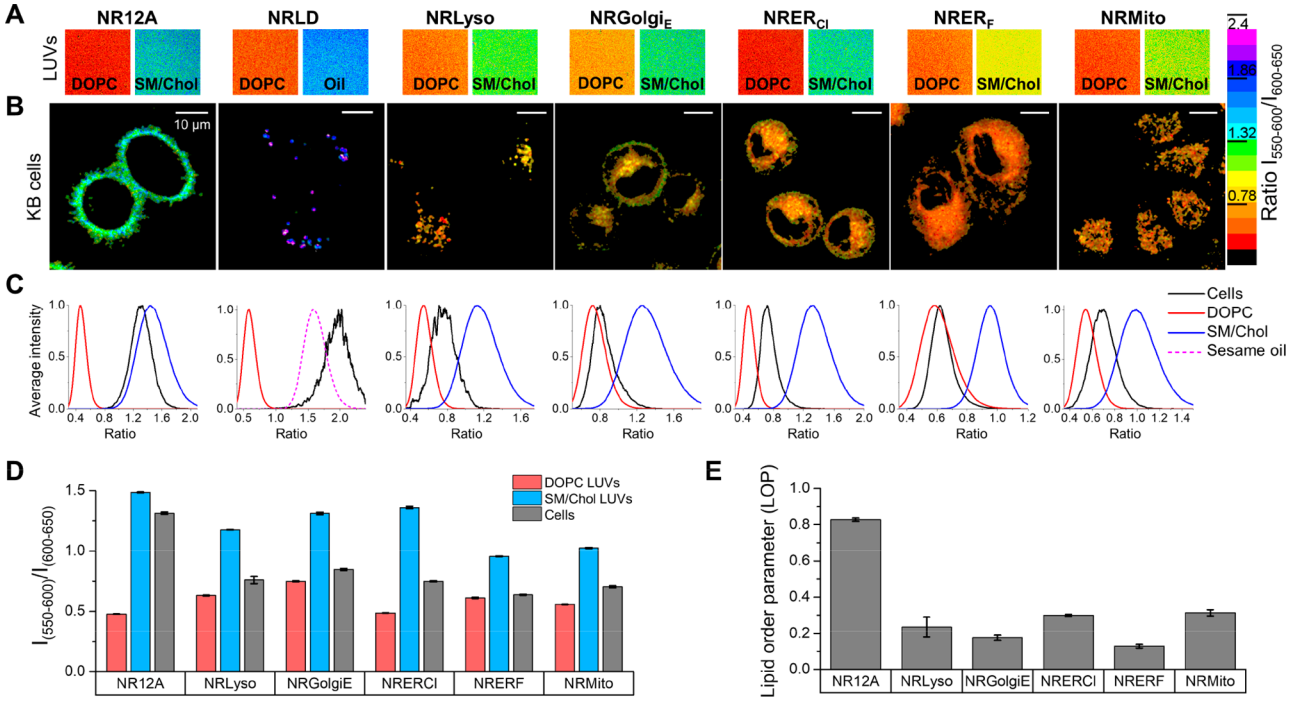

Figure 4. Solvatochromic organelle-specific probes reveal differences in polarity and lipid order within the organelles in KB cells. (A) Ratiometric confocal imaging of LUVs presenting Lo (DOPC) and Ld (SM/Chol) phases for calibration of the probes (in case of NRLD, sesame oil was used instead of the SM/Chol LUVs). Lipid and probe concentrations were 500 and 1 μM, respectively. (B) Ratiometric confocal imaging of KB cells by the solvatochromic organelle probes. Probe concentrations: 20 nM for NR12A; 50 nM for NRMito, NRLyso, NRLD, and NRER$_{Cl}$; 200 nM for NRER$_F$; 5 μM (in form of BSA-conjugate) for NRGolgi$_E$. (C) Distribution histograms of the green/red fluorescence intensity ratios ($I_{550-600}/I_{600-650}$) for corresponding probes in KB cells. (D) Weighted arithmetic mean values of the $I_{550-600}/I_{600-650}$ ratio obtained from LUVs and cell imaging data (A,B). (E) Lipid order parameter (LOP) calculated from ratiometric images of organelle probes in KB cells and LUVs under various conditions.

results suggest that all studied probes partition well into Ld phase, where they sense a less polar environment compared to water. A further blue shift of the band was systematically observed in the presence of cholesterol, showing their sensitivity to dehydration produced by cholesterol, similarly to Nile Red probes.[31] Much stronger effects were observed in SM/Chol LUVs, where the emission band shifted to the blue by 40−60 nm vs DOPC LUVs, similarly to parent Nile Red, indicating that the probes preserved the capacity to detect a much less polar/hydrated environment of the tightly packed Lo phase, in line with other solvatochromic dyes.[21] The exception was NRER$_F$, which showed a strong contribution of emission from the buffer with a blue-shifted shoulder corresponding to the Lo phase (Figure S2). The latter indicates that the probe is excluded from tightly packed Lo phase, probably due to the high bulkiness and/or polarity of its targeting moiety. Nevertheless, the blue-shifted shoulder suggests that the non-negligible fraction of the probe partitions into vesicles and identifies the low-polar environment of the Lo phase. Overall, the new probes can bind lipid membranes and

https://dx.doi.org/10.1021/jacs.0c10972
J. Am. Chem. Soc. XXXX, XXX, XXX−XXX

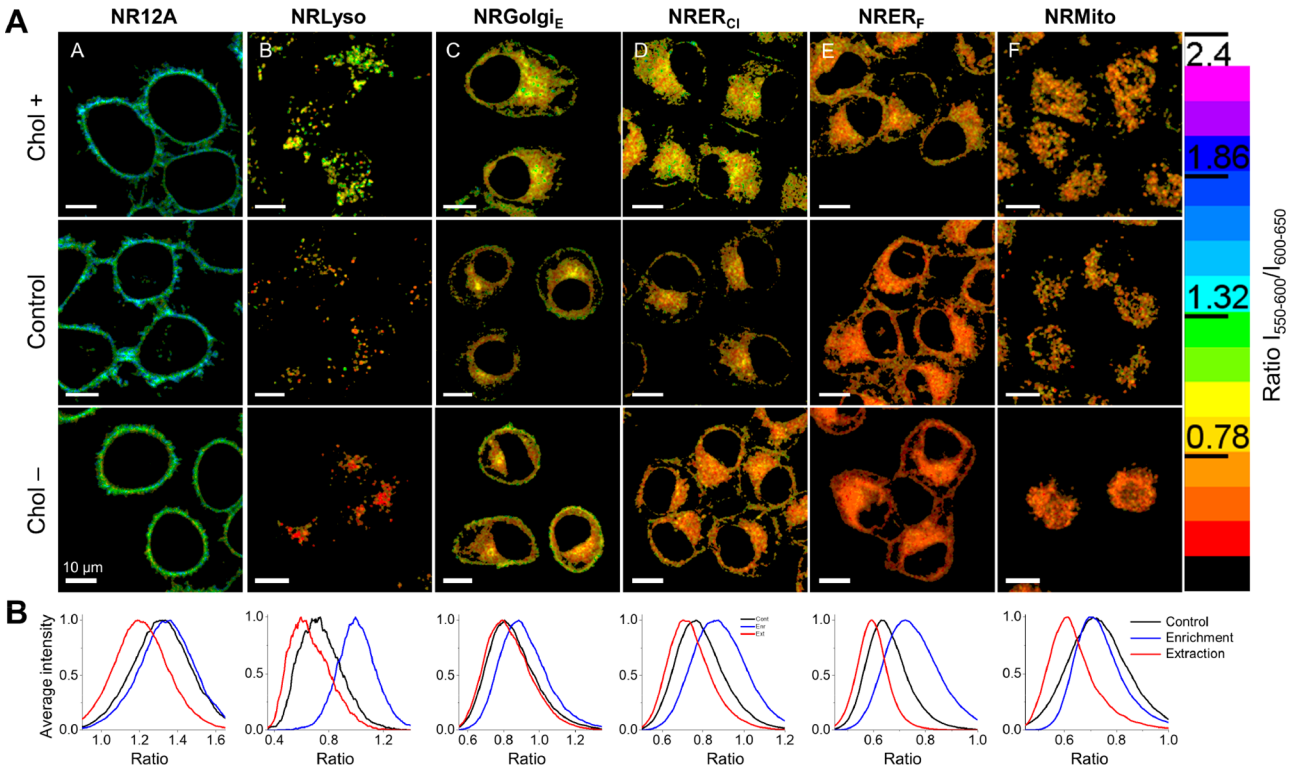

Figure 5. (A) Confocal ratiometric imaging of live KB cells with varied cholesterol content, using solvatochromic probes for organelles. Cholesterol enrichment (top panel) was produced by a saturated Chol/MBCD complex (3 h at 37 °C); cholesterol extraction (bottom panel) was produced by 5 mM MBCD (1 h at 37 °C). Probe concentrations: 20 nM for NR12A; 50 nM for NRMito, NRLyso, NRLD, and NRER$_{Cl}$; 200 nM for NRER$_F$; 5 μM (in form of BSA-conjugate) for NRGolgi$_E$. (B) Distribution histograms of the green/red fluorescence intensity ratios ($I_{550-600}/I_{600-650}$) for the corresponding probes in KB cells.

distinguish the Lo phase as much less polar compared to the Ld phase.

In order to evaluate the capacity of the probes to target a given organelle, we incubated them with live KB (Figure 3 and Figure S3) and HeLa (Figure S4) cells together with corresponding organelle markers. Importantly, each new probe showed significant colocalization with a corresponding commercial marker in both cells lines, having Pearson's correlation coefficient values in KB cells within the range from 0.89 to 0.96 (Table S2) (except NRGolgi$_E$ showing a bit lower values). The probe NRLyso in both cell lines exhibited an even higher selectivity compared to commercial LysoTracker Green, which is clear from the observed lower background noise in the images (Figure 3E and Figure S4E). Moreover, NRLD in HeLa cells showed a higher selectivity toward lipid droplets compared to the parent Nile Red dye (Figure S4G,H), which is probably because of a much higher hydrophobicity and bulky nature of the dicyclohexylamino group.

As the emission band position of Nile Red describes the local polarity and order of lipid structures, we analyzed this parameter by recording the short- and long-wavelength parts of the dye emission band below and above 600 nm and then constructed ratiometric images, in line with a previously used methodology.[43] Before cellular analysis, each probe was calibrated under a microscope in the model lipid membranes (LUVs) presenting the Lo and Ld phases, which correspond to extreme examples of order and disorder in lipid membranes. In the case of a NRLD probe, Lo phase vesicles were replaced with sesame oil, which was expected to mimic a non-polar environment in the oil core of LDs. Ratiometric fluorescence microscopy of LUVs (appeared as homogeneous signal, because individual vesicles cannot be resolved on this time scale) showed a drastic difference in the pseudocolor (Figure 4A) of the probes when Ld and Lo phases were compared. Indeed, the green/red fluorescence intensity ratio was systematically higher in the Lo phase, which corresponded to the blue shift in the emission spectra observed by spectroscopy (Figure 2 and Figure S2). Then, we analyzed the distribution of the green/red intensity ratio in the images (Figure 4C) and further obtained average ratio values (Figure 4D and Table S3), which allowed us to quantify the amplitude of the probe ratiometric response to Ld−Lo phase change. Both the ratio value and its variation in response to the phase change were characteristic for each probe, in line with the spectroscopy data above. Having our calibration data for Ld and Lo phases, we performed the ratiometric imaging of live KB cells (Figure 4B and Figure S5). Strikingly, the pseudocolor showed a dramatic variation in different organelles, which reflected strong differences in the green/red ratio (Figure 4C,D) and thus the local polarity. Indeed, the observed orange pseudocolor in the mitochondria and ER indicated the most polar microenvironment, whereas the blue-violet dots for lipid droplets and blue-green plasma membranes reflected a much lower local polarity (Figure 4B).

The local polarity detected by solvatochromic dyes reflects the lipid order in biomembranes: the higher the lipid order (and tighter lipid packing), the lower local polarity and hydration.[31] To interpret these local polarity variations in terms of lipid order, for each probe, we compared the green/red ratio in cells with that in our calibration images of LUVs (Figure 4C,D). While the ratio values for the plasma

https://dx.doi.org/10.1021/jacs.0c10972
J. Am. Chem. Soc. XXXX, XXX, XXX−XXX

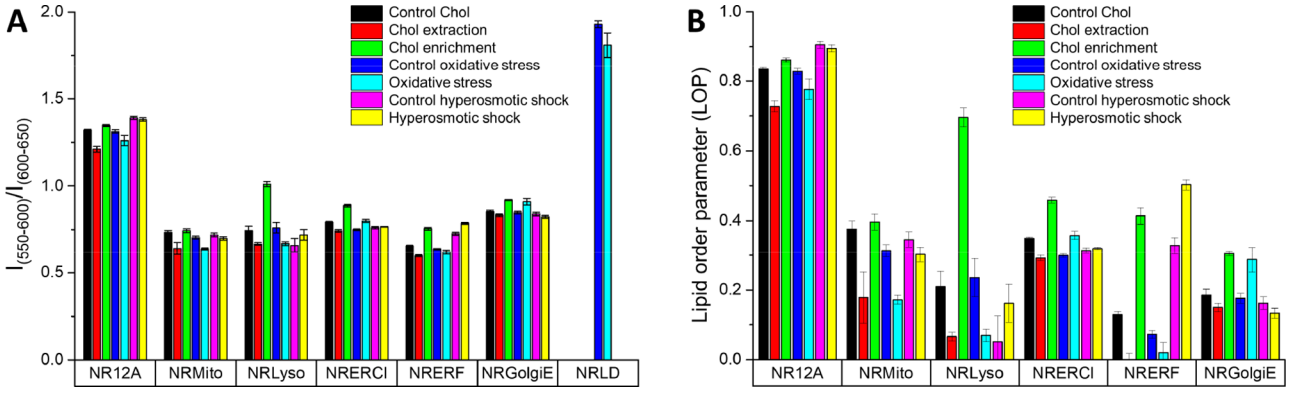

Figure 6. Quantitative analysis of fluorescence images of KB cells with solvatochromic probes for organelles after cholesterol extraction/enrichment, oxidative stress, and hyperosmotic shock. (A) Weighted arithmetic mean values of green/red fluorescence intensity ratios ($I_{550-600}/I_{600-650}$) and (B) lipid order parameter (LOP) values calculated from ratiometric images of organelle probes in KB cells and LUVs under various conditions.

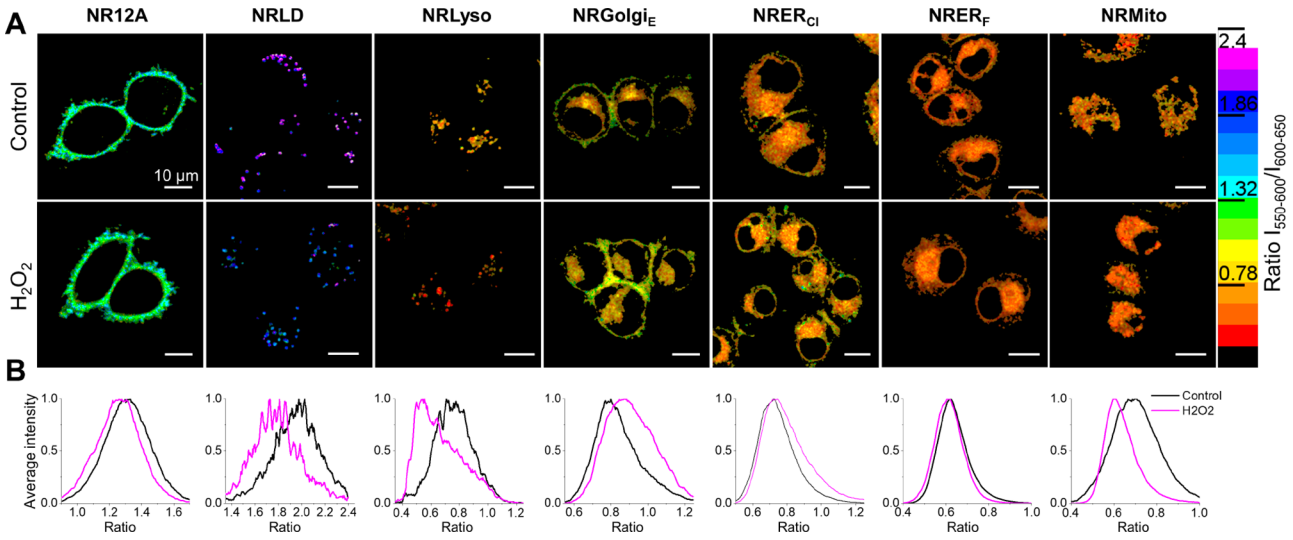

Figure 7. (A) Confocal ratiometric imaging of live KB cells under oxidative stress, using solvatochromic probes for organelles. The stress was produced by 2 mM hydrogen peroxide (1 h at 37 °C). Probe concentrations: 20 nM for NR12A; 50 nM for NRMito, NRLyso, NRLD, and $NRER_{Cl}$; 200 nM for $NRER_F$; 5 μM (in form of BSA-conjugate) for $NRGolgi_E$. (B) Distribution histograms of the green/red fluorescence intensity ratios ($I_{550-600}/I_{600-650}$) for the corresponding probes in KB cells.

membrane probe were close to those in Lo phase of LUVs, those for ER and Golgi ($NRER_F$ and $NRGolgi_E$) were close to those in Ld phase. To quantitatively describe the effects, we introduce a lipid order parameter, LOP = $(R - R_{DOPC})/(R_{SM/Chol} - R_{DOPC})$, which approaches 0 and 1, when the green/red ratio (R) is close to those in Ld (R_{DOPC}) and Lo ($R_{SM/Chol}$) phase LUVs, respectively (Figure 4E). According to this analysis, the plasma membranes presented the highest level of lipid order, close to that of SM/Chol, in line with earlier works.[42,43,49] Intracellular organelles displayed much lower LOP values, which decreased in the following order: NRMito ~ $NRER_{Cl}$ > NRLyso > $NRGolgi_E$ > $NRER_F$. The two probes, staining endoplasmic reticulum ($NRER_{Cl}$ and $NRER_F$), exhibited very different local lipid orders, possibly due to a much shallower insertion of the $NRER_F$ fluorophore inside the ER membrane. In the case of LDs, the LOP quantification was not applied, because the core−shell structure of LDs is different from lipid bilayers. The green/red ratio values for LDs (NRLD) were close to those in sesame oil (Figure 4C), reflecting a non-polar environment in the oil core of LDs.

Cholesterol is an essential component of biomembranes, distributing all over the cell.[9,12,13] Its excessive accumulation in cells is associated with a variety of diseases, including atherosclerosis[67] and Niemann-Pick C1 disease.[68] On the contrary, cholesterol extraction by treating the cells with methyl-β-cyclodextrin (MBCD)[69] leads to an impaired signal transduction due to disruption of lipid microdomains.[9,10] We applied our new probes to study the effects of cholesterol extraction and enrichment on biomembranes in different organelles. Cholesterol extraction produced significant changes in the ratiometric images (Figure 5A and Figure S6), corresponding to the decrease in the green/red ratio and the LOP values for all probes (Figures 5B and 6). Thus, our probes detected an increase in the local polarity associated with the loss of lipid order in all targeted organelles. This implies that the Nile Red fluorophore in all these probes is indeed inserted in the lipid membranes of corresponding organelles, which further validates our approach of organelle-specific lipid order sensing. Moreover, this result also confirms that cholesterol is distributed all over the cells and its removal affects the local membrane properties in all studied organelles. Importantly,

https://dx.doi.org/10.1021/jacs.0c10972
J. Am. Chem. Soc. XXXX, XXX, XXX−XXX

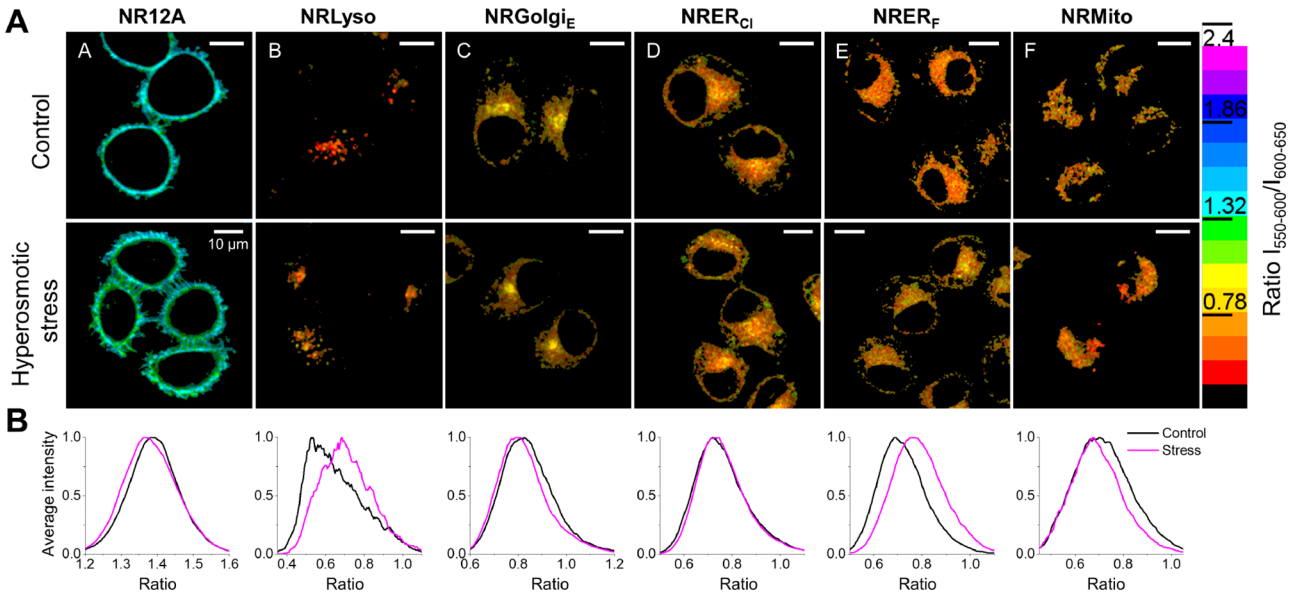

Figure 8. (A) Confocal ratiometric imaging of live KB cells under hyperosmotic shock, using solvatochromic probes for organelles. The shock was produced by replacing a half of the medium with 1 M sucrose solution. Probe concentrations: 20 nM for NR12A; 50 nM for NRMito, NRLyso, NRLD, and NRER$_{Cl}$; 200 nM for NRER$_F$; 5 μM (in form of BSA-conjugate) for NRGolgi$_E$. (B) Distribution histograms of the green/red fluorescence intensity ratios ($I_{550-600}/I_{600-650}$) for the corresponding probes in KB cells.

cholesterol enrichment using the MBCD/Chol complex produced the opposite effect, although the effect varied within the organelles. The increase in the green/red ratio and corresponding LOP values was particularly strong in the case of lysosomes and ER (Figure 6), initially characterized by a low lipid order and relatively low cholesterol content according to the literature data.[12] Thus, our probes reveal that cholesterol enrichment affects mostly the lipid order of the intracellular membranes with poor cholesterol content, in contrast to weakly affected plasma membranes, rich in cholesterol.

Exposing cells to hydrogen peroxide (H_2O_2) leads to an induction of oxidative stress, which is expected to alter the polarity of organelle membranes due to lipid peroxidation.[70] First, colocalization imaging experiments with reference organelle markers confirmed that the H_2O_2 treatment did not affect the organelle-specificity of the new probes (Figure S7, see Table S2 for Pearson's correlation coefficients). Second, after treatment with H_2O_2, the pseudocolor in ratiometric images (Figures 7A and S8) changed in a different way within the studied organelles, reflecting green/red ratio (*i.e.*, local polarity) changes (Figure 6). The most pronounced increase of polarity (decrease in the green/red ratio) was detected in case of LDs, lysosomes, and mitochondria (Figures 6 and 7B). A relatively high response in the case of LDs is in line with our previous results[34] indicating a high sensitivity of these organelles to oxidative stress, supposedly due to a large quantity of easily oxidizable unsaturated lipids. In the case of lysosomes, the treatment also resulted in a significant polarity increase, possibly because the interior of lysosomes derives from extracellular medium, and therefore, these organelles are highly exposed to the action of H_2O_2. The observed increase in heterogeneity of lysosomal polarity values (broadening of distribution of the intensity ratio, Figure 7B) is in line with the literature data.[71] The polarity increase in the mitochondria correlates well with the literature data concerning the high sensitivity of mitochondria to oxidative stress, which is directly linked to aging and apoptosis.[72,73] According to the LOP analysis, oxidative stress significantly decreased the lipid order in lysosomes and mitochondria, with LOP values reaching those after cholesterol extraction (Figure 6). The plasma membrane showed lower changes, supposedly due to a large quantity of saturated lipids, less prone to oxidation. NRER$_{Cl}$ and especially NRGolgi$_E$ showed a decrease in polarity in comparison to intact cells. In the case of NRGolgi$_E$, this decrease is unexpected and could be related to an increase in the fraction of saturated lipids and cholesterol because of oxidative stress. In addition, oxidative stress could alter the localization of the probe in the cells, even though they generally remain in the target organelles according to the colocalization data (see above). Overall, oxidative stress produced significant polarity/lipid order alternations in the membranes of the whole cell, with strongly varied responses in different organelles.

Mechanobiology is a rapidly growing research field that covers multiple aspects, including development,[74] collective cellular behavior,[75] tumor growth,[76] etc. As mechanical stress can directly affect the lipid order of biomembranes, the fluorescent tools sensitive to membrane tension and viscosity have been recently proposed to monitor mechanical stress at the level of organelles.[5,25,29] A simple method to induce mechanical stress in the cells is to change the osmolality of the media, for example by hyperosmotic stress, accompanied by the changes in lipid order and cell morphology.[66,77] Here, we studied the effect of hyperosmotic stress on organelles of live KB cells using our new probes for monitoring local polarity and lipid order. As in the case of oxidative stress, colocalization imaging experiments confirmed that hyperosmotic stress did not affect the organelle specificity of the new probes (Figure S9, see Table S2 for Pearson's correlation coefficients). The plasma membrane (stained with NR12A) upon the induction of hyperosmotic stress exhibited a change in morphology, yielding a jagged pattern together with the appearance of more polar (and less ordered) regions on the inner parts compared to the extremities (Figure 8 and Figure S10). This could be

https://dx.doi.org/10.1021/jacs.0c10972
J. Am. Chem. Soc. XXXX, XXX, XXX−XXX

attributed to the drop in lipid order in the most displaced parts of the membrane driven by cell shrinkage. These observations are in line with the previous results,[58] as these innermost parts of the plasma membrane seem to undergo more deformation, probably by stretching, compared to the outmost ones. In the cell extremities, the shrinkage is limited, probably due to the presence of rigid cytoskeleton filaments. Overall, the decrease in the LOP values (Figure 6) of PM reported by NR12A correlated with the decreased lipid order revealed by mechanosensitive flipper probe for PM.[5,29] A decrease in the LOP values (and increase in polarity) was also observed for mitochondria and Golgi apparatus, whereas lysosomes and ER showed the opposite effect (Figures 6 and 8). The observed lower LOP values in mitochondria membranes after hyperosmotic shock correlated well with the decrease in the lipid order and local viscosity reported by mitochondrial flipper[5] and molecular rotor[25] probes, respectively. It is also in line with a recent report on a solvatochromic mitochondria-specific probe.[54] The peculiar behavior of lysosomes (e.g., lower polarity and higher LOP) is probably because they are expected to shrink, which induces a higher lipid ordering at the inner leaflet of the vesicles, where NRLyso locates. It should be noted that the green/red intensity ratio of the probes in plasma membranes, lysosomes, and ER ($NRER_F$) (Figure 6A) varied within the control cells of different cell culture passages (cells in Figure 8 were ∼8 passages older than those in Figure 7 and ∼13 passages older than those in Figure 5). This interesting effect would require a dedicated study in order to verify whether the polarity and lipid order of these biomembranes are also affected by cell aging. The two probes for ER yielded a different response toward hyperosmotic stress: practically no response from $NRER_{Cl}$, in contrast to a pronounced increase in the LOP values (and decrease in polarity) reported by $NRER_F$ (Figures 6 and 8). As $NRER_F$, bearing a polar PEG linker, is poorly inserted into the lipid membrane according to data in LUVs (Figure S2), the cell shrinkage during hyperosmotic stress produces a compaction of ER, which can force deeper insertion of the Nile Red moiety into the ER membranes. This result is in line with the previously reported increase in the local viscosity revealed by molecular rotors targeted to ER,[25] although in this case the ER flipper probe showed some decrease in the lipid order.[5] Overall, mechanical stress in cells produced very different responses within the organelles, probably because of different geometry and lipid compositions of their membranes as well as different locations of the probe within the bilayer leaflets and varied insertion of their fluorophore.

CONCLUSIONS

In this work, we synthesized an array of organelle-targeted solvatochromic fluorescent probes based on Nile Red. Overall, the developed probes for ER, mitochondria, Golgi apparatus, lipid droplets, lysosomes, and plasma membrane (from an earlier report[58]) are capable of selective organelle targeting with sensing of the local polarity, revealing fine differences in their lipid order. As we used the same solvatochromic dye, it became possible to directly compare the local polarity for different organelles and thus establish the following trend: lipid droplets ≪ plasma membrane ≪ Golgi apparatus < lysosomes < ER < mitochondria < ER (with shallow probe $NRER_F$). However, each probe, having different chemical designs, reported slightly different local polarities even for the same model lipid membrane, as evidenced by spectroscopy and microscopy data in lipid vesicles. Therefore, to directly compare the lipid order in different organelles, we developed a methodology to convert the observed local polarity into a quantitative lipid order parameter, using a calibration of each probe in model lipid bilayers of ordered and disordered phases. This approach allowed us to establish the first quantitative comparison of lipid order in biomembranes of different organelles, revealing the following trend, slightly different from that based on local polarity: plasma membrane ≫ mitotochondria ∼ ER > lysosomes > Golgi apparatus > ER (with shallow probe $NRER_F$). All new probes showed a ratiometric response to cholesterol depletion and enrichment, thus confirming that the probes sense a lipid order in the biomembranes of the studied organelles. Moreover, the effect of cholesterol enrichment was particularly strong in cholesterol-poor organelles, such as ER and lysosomes, in contrast to cholesterol-rich plasma membranes where the effect was very small.

The toolkit of solvatochromic probes revealed that organelles are differently sensitive to oxidative or hyperosmotic stress in terms of their local polarity and lipid order: lipid droplets, mitochondria, and lysosomes being the most sensitive toward oxidative stress, where a significant polarity increase was observed, probably due to a modification of fatty acid chains with polar superoxide groups. On the contrary, lysosomes, ER (with a shallow probe), and mitochondria showed the strongest response to hyperosmotic conditions. Moreover, hyperosmotic stress increased the heterogeneity in the plasma membrane, possibly due to an appearance of liquid disordered phase domains presumably at the places with the highest mechanical stress. Overall, the new solvatochromic probes enable the deciphering of fine changes in the local polarity and lipid order specifically in different organelles. However, special care should be taken with the fluorophore insertion into the bilayer controlled by polarity and bulkiness of the targeting group, because it may significantly alter the probe response. Even though the Nile Red moiety in these probes is lipophilic and preferentially localizes in lipid membranes, one cannot totally exclude an additional effect of membrane proteins, including those translocating between the membrane and lumen of an organelle.

The changes observed in organelles under mechanical stress by our solvatochromic probes correlate with those reported earlier by viscosity-sensitive molecular rotors and mechanosensitive flippers, although some differences have also been noticed. On the one hand, for all these three types of probes, the increase in lipid order produces profound changes in the bilayer, increasing viscosity and rigidity, while decreasing local polarity. On the other hand, different stress conditions (e.g., chemical and mechanical) could produce different effects on those three membrane parameters. Systematic work on comparing these three families of probes will be needed to better understand the fine differences in their response profiles. Overall, the present work highlights the importance of the use of the same fluorophore in the design of probes for studying and comparing properties of different target organelles. Moreover, it proposes an approach for the quantitative comparison of the local lipid order in organelles, on the basis of the calibration of probes in model vesicles with a defined lipid order. Finally, this work proposes a toolkit of probes that can be directly used in cell biology, mechanobiology, and biophysics for shedding light on the behavior of cellular organelles and their response to external stress.

https://dx.doi.org/10.1021/jacs.0c10972
J. Am. Chem. Soc. XXXX, XXX, XXX−XXX

EXPERIMENTAL SECTION

General Methods and Materials. All the reagents were purchased from Sigma-Aldrich, Alfa Aesar, or TCI and used as received. Milli-Q-water (Millipore) was used in all experiments. NMR spectra were recorded at 20 °C on a Bruker Avance III 400 spectrometer. Mass spectra were obtained using an Agilent Q-TOF 6520 mass spectrometer. Absorption spectra were recorded on a Cary 4000-HP spectrophotometer (Varian), and emission spectra were recorded on a Fluoromax 4 (Jobin Yvon, Horiba) spectrofluorometer equipped with a thermostated cell compartment. Fluorescence quantum yields were measured using Nile Red (NR) in methanol (λ_{ex}= 520 nm, QY_{ref} = 38%)[78] as a reference. Compounds **1** and **NR12A** were synthesized according to the previously published procedure.[58]

(3-(4-(Ethyl(5-oxo-5*H*-benzo[*a*]phenoxazin-9-yl)amino)-butanamido)propyl)triphenylphosphonium (NRMito). Compound **1** (30 mg) was dissolved in 1 mL of dry DMF together with 31.9 mg (1.05 equiv) of HATU, 5.4 mg (0.5 equiv) of HOBt, and 61.9 mg (6 equiv, 84 μL) of DIPEA under an Ar atmosphere. After 5 min, a solution of 40.3 mg (1.05 equiv) of 3-aminopropyltriphenylphosphonium bromide in 1 mL of dry DMF was added, and the mixture was stirred for 24 h (control by TLC) under an Ar atmosphere. After the reaction, the solvent was evaporated *in vacuo* and the product was purified by preparative TLC (SiO_2, DCM/MeOH 92:8). After the TLC, the traces of DMF were removed by washing the crystalline product on a filter twice with diethyl ether and drying. Yield: 26 mg (43.0%) as a dark red solid. ^{1}H NMR (400 MHz, $CDCl_3$): δ 8.66 (d, *J* = 7.5 Hz, 1H), 8.31 (dd, *J* = 7.8, 1.0 Hz, 1H), 7.58−7.82 (m, 18H), 6.86 (br t, *J* = 6.0 Hz, 1H), 6.76 (dd, *J* = 9.2, 2.6 Hz, 1H), 6.57 (d, *J* = 2.5 Hz, 1H), 6.36 (s, 1H), 3.37−3.54 (m, 6H), 3.16−3.27 (m, 2H), 2.38 (br t, *J* = 7.0 Hz, 2H), 1.86−2.02 (m, 4H), 1.25 (t, *J* = 7.0 Hz, 3H) ppm. ^{13}C NMR (101 MHz, $CDCl_3$): δ 183.66 (C_{ar}), 173.59 (C_{amide}), 152.16 (C_{ar}), 151.12 (C_{ar}), 146.68 (C_{ar}), 139.53 (C_{ar}), 135.37 (C_{ar}), 133.24 (d, *J* = 10.0 Hz, C_{ar}), 132.07 (C_{ar}), 131.65 (C_{ar}), 131.22 (d, *J* = 11.4 Hz, C_{ar}), 130.64 (d, *J* = 12.65 Hz, C_{ar}), 129.79 (C_{ar}), 125.57 (C_{ar}), 125.01 (C_{ar}), 123.75 (C_{ar}), 118.15 (C_{ar}), 117.29 (C_{ar}), 110.15 (C_{ar}), 105.48 (C_{ar}), 96.42 (C_{ar}), 50.22 (C_{al}), 45.56 (C_{al}), 39.14 (d, *J* = 17.8 Hz, C_{al}), 32.82 (C_{al}), 23.25 (C_{al}), 22.49 (d, *J* = 3.5 Hz, C_{al}), 20.17 (d, *J* = 53.5 Hz, C_{al}), 12.36 (s, C_{al}) ppm. HRMS (ESI), *m*/*z*: $[M]^+$ calcd for $C_{43}H_{41}N_3O_3P$, 678.2880; found, 678.2889.

4-(Ethyl(5-oxo-5*H*-benzo[*a*]phenoxazin-9-yl)amino)-*N*-(3-morpholinopropyl)butanamide (NRLyso). Compound **1** (30 mg) was dissolved in 2 mL of dry DMF together with 31.9 mg (1.05 equiv) of HATU, 5.4 mg (0.5 equiv) of HOBt, and 41.2 mg (4 equiv, 56 μL) of DIPEA under an Ar atmosphere. After 5 min, 12.1 mg (1.05 equiv, 12.2 μL) of 3-morpholinopropylamine was added, and the mixture was stirred for 24 h (control by TLC) under an Ar atmosphere. After the reaction, the solvent was evaporated *in vacuo* and the crude product was purified by preparative TLC (two consecutive purifications, SiO_2; DCM/MeOH 90:10). Yield: 6 mg (15.0%) as a dark red solid. ^{1}H NMR (400 MHz, $CDCl_3$): δ 8.63 (dd, *J* = 8.2, 1.1 Hz, 1H), 8.29 (dd, *J* = 7.8, 1.0 Hz, 1H), 7.72 (td, *J* = 8.0, 1.8 Hz, 1H), 7.65 (td, *J* = 7.8, 1.0 Hz, 1H), 7.58 (d, *J* = 9.3 Hz, 1H), 7.07 (br t, *J* = 4.5 Hz, 1H), 6.69 (dd, *J* = 9.3, 2.8 Hz, 1H), 6.49 (d, *J* = 2.8 Hz, 1H), 6.36 (s, 1H), 3.68 (t, *J* = 4.6 Hz, 4H), 3.42−3.52 (m, 4H), 3.39 (q, *J* = 6.0 Hz, 2H), 2.38−2.51 (m, 6H), 2.26 (t, *J* = 7.0 Hz, 2H), 2.00 (quin, *J* = 7.3 Hz, 2H), 1.70 (quin, *J* = 6.3 Hz, 2H), 1.25 (t, *J* = 7.2 Hz, 3H) ppm. ^{13}C NMR (101 MHz, DMSO-d_6): δ 183.76 (C_{ar}), 171.60 (C_{amide}), 152.10 (C_{ar}), 150.97 (C_{ar}), 146.65 (C_{ar}), 140.11 (C_{ar}), 132.04 (C_{ar}), 131.72 (C_{ar}), 131.35 (C_{ar}), 131.12 (C_{ar}), 129.97 (C_{ar}), 125.65 (C_{ar}), 125.03 (C_{ar}), 123.83 (C_{ar}), 109.91 (C_{ar}), 105.72 (C_{ar}), 96.54 (C_{ar}), 67.05 (C_{al}), 57.81 (C_{al}), 53.68 (C_{al}), 49.95 (C_{al}), 45.44 (C_{al}), 39.45 (C_{al}), 33.18 (C_{al}), 24.93 (C_{al}), 23.20 (C_{al}), 12.35 (C_{al}) ppm. HRMS (ESI), *m*/*z*: $[M + H]^+$ calcd for $C_{29}H_{35}N_4O_4$, 503.2659; found, 503.2679.

***tert*-Butyl(1-oxo-1-(perfluorophenyl)-5,8,11,14,17,20,23,26,29,32,35-undecaoxa-2-azaheptatriacontan-37-yl)carbamate (2a).** BocHN-PEG_{11}-NH_2 (260 mg) was dissolved in 5 mL of dry DCM together with 730 mg (5.5 equiv) of Cs_2CO_3, and the mixture was cooled to 0 °C in an ice bath. Then, 415 mg (4.5 equiv, 260 μL) of pentafluorobenzoyl chloride was added, and the mixture was stirred for 1 h at 0 °C and then for 1 h at room temperature under an Ar atmosphere. After the reaction, the solvent was evaporated *in vacuo* and then 98.7 μL of TFA together with 10 mL of DCM was added to neutralize Cs_2CO_3. After this, the solid residue was filtered off and the solvent was evaporated *in vacuo*. The crude product was purified by column chromatography (SiO_2; DCM/MeOH 95:5, alkaline $KMnO_4$ staining for TLC analysis of the column fractions). Yield: 259 mg (76.6%) as a colorless oil. ^{1}H NMR (400 MHz, $CDCl_3$): δ 7.09 (br s, 1H), 5.04 (br s, 1H), 3.55−3.69 (m, 44H), 3.53 (br t, *J* = 5.1 Hz, 1H), 3.30 (br q, *J* = 5.0 Hz, 2H), 2.43 (br s, 1H), 1.43 (s, 9H) ppm. ^{13}C NMR (101 MHz, DMSO-d_6): δ 157.44 (C_{carbox}), 156.00 (C_{carbox}), 145.29 (C_{ar}), 142.83 (C_{ar}), 138.81 (C_{ar}), 136.27 (C_{ar}), 112.04 (d, *J* = 3.7 Hz, C_{ar}), 78.71−79.49 (m, C_{al}), 70.48−70.62 (m, C_{al}), 70.47 (C_{al}), 70.45 (C_{al}), 70.43 (C_{al}), 70.37 (C_{al}), 70.26 (C_{al}), 70.21 (C_{al}), 69.35 (C_{al}), 40.38 (C_{al}), 40.15 (C_{al}), 28.41 (C_{al}) ppm. HRMS (ESI), *m*/*z*: $[M + Na]^+$ calcd for $C_{36}H_{59}F_5N_2O_{14}Na$, 861.3786; found, 861.3807.

***N*-(35-Amino-3,6,9,12,15,18,21,24,27,30,33-undecaoxapentatriacontyl)-2,3,4,5,6-pentafluorobenzamide (2b).** Compound **1a** (240 mg) was dissolved in 2 mL of dry DCM; after that, 2 mL of TFA was added and the mixture was stirred for 2 h at room temperature. After the reaction, the solvent was evaporated *in vacuo*. In order to eliminate traces of TFA, 1 mL of methanol was added, followed by evaporation *in vacuo* (three times). Yield: 238 mg (97.2%) as a colorless oil. ^{1}H NMR (400 MHz, $CDCl_3$): δ 7.43 (br s, 1H), 7.02 (br s, 1H), 3.78 (t, *J* = 5.3 Hz, 2H), 3.58−3.71 (m, 44H), 3.15 (sxt, *J* = 5.4 Hz, 2H) ppm. ^{13}C NMR (101 MHz, DMSO-d_6): δ 176.96 (C_{amide}), 159.68 (q, *J* = 39.40 Hz, C_{ar}), 158.36 (C_{ar}), 115.33 (q, *J* = 287.69 Hz, C_{ar}), 70.26 (C_{al}), 70.23 (C_{al}), 70.15 (C_{al}), 70.12 (C_{al}), 70.09 (C_{al}), 70.04 (C_{al}), 70.01 (C_{al}), 69.89 (C_{al}), 69.84 (C_{al}), 69.79 (C_{al}), 69.78 (C_{al}), 69.74 (C_{al}), 69.70 (C_{al}), 69.63 (C_{al}), 69.55 (C_{al}), 69.41 (C_{al}), 69.16 (C_{al}), 66.64 (C_{al}), 40.13 (C_{al}), 39.78 (C_{al}), 21.97 (C_{al}) ppm. HRMS (ESI), *m*/*z*: $[M + H]^+$ calcd for $C_{31}H_{52}F_5N_2O_{12}$, 739.3441; found, 739.3471.

2,3,4,5,6-Pentafluoro-*N*-(37-oxo-41-(5-oxo-5*H*-benzo[*a*]-phenoxazin-9-yl)-6,9,12,15,18,21,24,27,30,33-undecaoxa-36,41-diazatritetracontyl)benzamide ($NRER_F$). Compound **1** (30 mg) was dissolved in 1 mL of dry DMF together with 31.9 mg (1.05 equiv) of HATU, 5.4 mg (0.5 equiv) of HOBt, and 61.9 mg (6 equiv, 84 μL) of DIPEA under an Ar atmosphere. After 5 min, a solution of 71.4 mg (1.05 equiv) of **2b** in 1 mL of dry DMF was added, and the mixture was stirred for 24 h (control by TLC) under an Ar atmosphere. After the reaction, the solvent was evaporated *in vacuo*. The crude product was purified by preparative TLC (SiO_2, DCM/MeOH 95:5). Yield: 53 mg (60.6%) as a dark red oil. ^{1}H NMR (400 MHz, $CDCl_3$): δ 8.62 (d, *J* = 7.5 Hz, 1H), 8.25 (d, *J* = 7.5 Hz, 1H), 7.70 (td, *J* = 7.53, 1.2 Hz, 1H), 7.62 (td, *J* = 7.53, 1.2 Hz, 1H), 7.57 (d, *J* = 9.3 Hz, 1H), 7.32−7.40 (m, 1H), 6.70 (dd, *J* = 9.0, 2.5 Hz, 1H), 6.56 (br t, *J* = 4.5 Hz, 1H), 6.49 (d, *J* = 2.5 Hz, 1H), 6.35 (s, 1H), 3.55−3.69 (m, 44H), 3.39−3.50 (m, 8H), 2.30 (br t, *J* = 7.0 Hz, 2H,) 1.98 (quin, *J* = 7.3 Hz, 2H), 1.23 (t, *J* = 7.0 Hz, 3H) ppm. ^{13}C NMR (101 MHz, DMSO-d_6): δ 183.73 (C_{ar}), 172.34 (C_{amide}), 157.63 (C_{amide}), 152.18 (C_{ar}), 151.09 (C_{ar}), 146.68 (C_{ar}), 145.29 (C_{ar}), 142.74 (C_{ar}), 139.71 (C_{ar}), 138.77 (C_{ar}), 136.28 (C_{ar}), 132.05 (C_{ar}), 131.62 (C_{ar}), 131.33 (C_{ar}), 131.17 (C_{ar}), 129.86 (C_{ar}), 125.57 (C_{ar}), 125.09 (C_{ar}), 123.79 (C_{ar}), 112.09 (d, *J* = 3.7 Hz, C_{ar}), 110.11 (C_{ar}), 105.52 (C_{ar}), 96.46 (C_{ar}), 70.41 (C_{al}), 70.35 (C_{al}), 70.28 (C_{al}), 70.27 (C_{al}), 70.21 (C_{al}), 70.18 (C_{al}), 70.07 (C_{al}), 69.89 (C_{al}), 69.42 (C_{al}), 50.64 (C_{al}), 50.09 (C_{al}), 45.50 (C_{al}), 40.11 (C_{al}), 39.26 (C_{al}), 32.86 (C_{al}), 23.13 (C_{al}), 12.35 (C_{al}) ppm. HRMS (ESI), *m*/*z*: $[M + Na]^+$ calcd for $C_{53}H_{69}F_5N_4O_{15}Na$, 1119.4580; found, 1119.4619.

***N*-(3-Chloropropyl)-4-(ethyl(5-oxo-5*H*-benzo[*a*]phenoxazin-9-yl)amino)butanamide ($NRER_{Cl}$).** Compound **1** (30 mg) was dissolved in 1 mL of dry DMF together with 31.9 mg (1.05 equiv) of HATU, 5.4 mg (0.5 equiv) of HOBt, and 61.9 mg (6 equiv, 84 μL) of DIPEA under an Ar atmosphere. After 5 min, a solution of 10.9 mg (1.05 equiv) of 3-chloropropylamine in 1 mL of dry DMF was added, and the mixture was stirred for 24 h (control by TLC) under an Ar

https://dx.doi.org/10.1021/jacs.0c10972
J. Am. Chem. Soc. XXXX, XXX, XXX−XXX

atmosphere. After the reaction, the solvent was evaporated *in vacuo* and then the solid residue was dissolved in EtOAc, washed with water (×3), and dried over Na_2SO_4, and the solvent was evaporated *in vacuo*. The crude product was purified by preparative TLC (SiO_2, DCM/MeOH 98:2). Yield: 14 mg (38.9%) as a dark red solid. ^{1}H NMR (400 MHz, $CDCl_3$): δ 8.61 (dd, J = 8.0, 0.8 Hz, 1H), 8.22 (dd, J = 7.9, 0.9 Hz, 1H), 7.70 (td, J = 7.6, 1.3 Hz, 1H), 7.62 (td, J = 7.6, 1.0 Hz, 1H), 7.54 (d, J = 9.0 Hz, 1H), 6.68 (dd, J = 9.0, 2.8 Hz, 1H), 6.48 (d, J = 2.8 Hz, 1H), 6.32 (s, 1H), 6.24 (br t, J = 5.8 Hz, 1H), 3.59 (t, J = 6.4 Hz, 2H), 3.37−3.50 (m, 6H), 2.31 (t, J = 7.2 Hz, 2H), 1.94−2.06 (m, 4H), 1.22 (t, J = 7.2 Hz, 3H) ppm. ^{13}C NMR (101 MHz, DMSO-d_6): δ 183.77 (C_{ar}), 172.50 (C_{amide}), 152.38 (C_{ar}), 151.24 (C_{ar}), 146.71 (C_{ar}), 139.33 (C_{ar}), 132.09 (C_{ar}), 131.51 (C_{ar}), 131.42 (C_{ar}), 131.25 (C_{ar}), 129.83 (C_{ar}), 125.45 (C_{ar}), 125.32 (C_{ar}), 123.89 (C_{ar}), 110.33 (C_{ar}), 105.19 (C_{ar}), 96.45 (C_{ar}), 55.60 (C_{al}), 50.07 (C_{al}), 45.52 (C_{al}), 37.17 (C_{al}), 33.09 (C_{al}), 32.15 (C_{al}), 23.25 (C_{al}), 12.36 (C_{al}) ppm. HRMS (ESI), m/z: $[M - H - Cl + Na]^+$ calcd for $C_{25}H_{25}N_3O_3Na$, 438.1796; found, 438.1802.

***tert*-Butyl(2-dodecanamidoethyl)carbamate (3a).** Myristic acid (0.5 g) was dissolved in 5 mL of dry DMF together with 874 mg (1.05 equiv) of HATU, 148 mg (0.5 equiv) of HOBt, and 850 mg (3 equiv, 1.15 mL) of DIPEA under an Ar atmosphere. After 5 min, a solution of 368 mg (1.05 equiv) of *N*-Boc-ethylenediamine in 5 mL of dry DMF was added, and the mixture was stirred for 24 h (control by TLC). After the reaction, the solvent was evaporated *in vacuo* and the product was purified by column chromatography (SiO_2, DCM/MeOH 95:5). Yield: 670 mg (80.6%) as a pale yellowish solid. ^{1}H NMR (400 MHz, $CDCl_3$): δ 6.10 (br s, 1H), 4.88 (br s, 1H), 3.32−3.39 (m, 2H), 3.22−3.31 (m, 2H), 2.16 (t, J = 8.0 Hz, 2H), 1.61 (m, 4H), 1.44 (s, 9H), 1.20−1.34 (m, 18H), 0.88 (t, J = 6.8 Hz, 3H) ppm.

***N*-(2-Aminoethyl)dodecanamide (3b).** Compound **3a** (240 mg) was dissolved in 2 mL of dry DCM; after that, 2 mL of TFA was added and the mixture was stirred for 2 h at room temperature. After the reaction, the solvent was evaporated *in vacuo*. In order to eliminate traces of TFA, 1 mL of methanol was added, followed by evaporation *in vacuo* (three times). Yield: 241.9 mg (97.0%) (in a form of TFA salt) as a pale yellowish solid. ^{1}H NMR (400 MHz, $CDCl_3$): δ 7.37 (br s, 1H), 3.45−3.58 (m, 2H), 3.05−3.21 (m, 2H), 1.48−1.61 (m, 2H), 1.17−1.33 (m, 20H), 0.87 (t, J = 7.0 Hz, 3H) ppm.

***N*-(2-(4-(Ethyl(5-oxo-5*H*-benzo[*a*]phenoxazin-9-yl)amino)-butanamido)ethyl)tetradecanamide (NRGolgi$_E$).** Compound **1** (30 mg) was dissolved in 1 mL of dry DMF together with 31.9 mg (1.05 equiv) of HATU, 5.4 mg (0.5 equiv) of HOBt, and 41.23 mg (4 equiv, 55.6 μL) of DIPEA under an Ar atmosphere. After 5 min, a solution of 22.7 mg (1.05 equiv) of **3b** and 28 μL of DIPEA in 1 mL of dry DCM was added, and the mixture was stirred for 24 h (control by TLC) under an Ar atmosphere. After the reaction, the solvent was evaporated *in vacuo* and the crude product was separated by preparative TLC. Yield: 22 mg (43.9%) as a dark red solid. ^{1}H NMR (400 MHz, $CDCl_3$): δ 8.63 (d, J = 7.8 Hz, 1H), 8.25 (d, J = 7.8 Hz, 1H), 7.71 (td, J = 7.5, 1.0 Hz, 1H), 7.63 (br td, J = 7.5, 1.0 Hz, 1H), 7.56 (d, J = 9.0 Hz, 1H), 6.82 (br s, 1H), 6.69 (dd, J = 9.0, 2.5 Hz, 1H), 6.46−6.53 (m, 2H), 6.35 (s, 1H), 3.35−3.52 (m, 8H), 2.31 (t, J = 7.3 Hz, 2H), 2.18 (t, J = 7.7 Hz, 2H), 1.93−2.03 (m, 2H), 1.53−1.63 (m, 2H), 1.16−1.32 (m, 23H), 0.87 (t, J = 6.9 Hz, 3H) ppm. The ^{13}C NMR spectra could not be obtained due to limited solubility of the probe. HRMS (ESI), m/z: $[M + Na]^+$ calcd for $C_{38}H_{52}N_4O_4Na$, 651.3889; found, 651.3902.

***N*,*N*-Dicyclohexyl-4-(ethyl(5-oxo-5*H*-benzo[*a*]phenoxazin-9-yl)amino)butanamide (NRLD).** Compound **1** (30 mg) was dissolved in 1 mL of dry DMF together with 31.9 mg (1.05 equiv) of HATU, 5.4 mg (0.5 equiv) of HOBt, and 51 mg (5 equiv, 70 μL) of DIPEA under an Ar atmosphere. After 5 min, a solution of 15.2 mg (1.05 equiv, 16.7 μL) of dicyclohexylamine in 1 mL of dry DMF was added, and the mixture was stirred for 24 h (control by TLC) under an Ar atmosphere. After the reaction, the solvent was evaporated *in vacuo* and the solid residue was dissolved in DCM, washed with water and brine, and dried over Na_2SO_4, and then, the solvent was evaporated *in vacuo*. The crude product was purified by preparative TLC (two consecutive purifications, SiO_2; DCM/MeOH 99:1 and SiO_2; DCM/MeOH 98:2, respectfully). Yield: 30 mg (67.5%) as a dark red solid. ^{1}H NMR (400 MHz, $CDCl_3$): δ 8.63 (dd, J = 8.0, 0.8 Hz, 1H), 8.29 (dd, J = 7.8, 1.0 Hz, 1H), 7.71 (td, J = 7.5, 1.5 Hz, 1H), 7.63 (td, J = 7.5, 1.5 Hz, 1H), 7.58 (d, J = 9.0 Hz, 1H), 6.70 (dd, J = 9.3, 2.8 Hz, 1H), 6.50 (d, J = 2.8 Hz, 1H), 6.36 (s, 1H), 3.43−3.51 (m, 5H), 2.40−2.60 (m, 2H), 2.36 (t, J = 6.5 Hz, 2H), 1.97 (quin, J = 7.0 Hz, 2H), 1.76−1.87 (m, 4H), 1.59−1.70 (m, 4H), 1.46−1.57 (m, 4H), 1.03−1.33 (m, 10H) ppm. ^{13}C NMR (101 MHz, DMSO-d_6): δ 183.72 (C_{ar}), 170.60 (C_{amide}), 152.14 (C_{ar}), 151.17 (C_{ar}), 146.69 (C_{ar}), 139.91 (C_{ar}), 132.07 (C_{ar}), 131.74 (C_{ar}), 131.27 (C_{ar}), 131.08 (C_{ar}), 129.87 (C_{ar}), 125.66 (C_{ar}), 124.99 (C_{ar}), 123.76 (C_{ar}), 109.97 (C_{ar}), 105.67 (C_{ar}), 96.52 (C_{ar}), 50.10 (C_{al}), 45.40 (C_{al}), 30.22 (C_{al}), 26.66 (C_{al}), 26.09 (C_{al}), 25.42 (C_{al}), 25.23 (C_{al}), 22.99 (C_{al}), 12.36 (C_{al}) ppm. HRMS (ESI), m/z: $[M + Na]^+$ calcd for $C_{22}H_{20}N_2O_4Na$, 562.3048; found, 562.3062.

Preparation of Liposomes. All types of large unilamellar vesicles (LUVs) used were prepared by the following procedure. A stock solution of corresponding lipid(s) in chloroform was placed into a round-neck flask, after which the solvent was evaporated *in vacuo* and phosphate buffer (20 mM, pH 7.4) was added. After all of the solid had dissolved, a suspension of multilamellar vesicles was extruded by using a Lipex Biomembranes extruder (Vancouver, Canada). The size of the filters was first 0.2 μm (7 passages) and thereafter 0.1 μm (10 passages). This generates monodisperse LUVs with a mean diameter of 0.12 μm, as measured with a Malvern Zetamaster 300 (Malvern, U.K.). The phospholipid/cholesterol molar ratio in the case of DOPC/Chol and Sphing/Chol was 1:0.9.

Cell Lines, Culture Conditions, and Treatment. HeLa cells (ATCC CCL-2) cells were grown in Dulbecco's modified eagle medium (DMEM, Gibco Invitrogen), supplemented with 10% fetal bovine serum (FBS, Lonza), 1% L-glutamine (Sigma-Aldrich), and 1% antibiotic solution (penicillin−streptomycin, Gibco-Invitrogen) at 37 °C in a humidified 5% CO_2 atmosphere. KB (ATCC CCL-17) cells were grown in Dulbecco's modified eagle medium (DMEM, Gibco Invitrogen) and supplemented with 10% fetal bovine serum (FBS, Lonza), 1% L-glutamine (Sigma-Aldrich), 1% non-essential amino acid solution (Gibco-Invitrogen), and 1% MEM vitamin solution (Gibco-Invitrogen) at 37 °C in a humidified 5% CO_2 atmosphere. Cells were seeded onto a chambered coverglass (IBIDI) at a density of 5 × 10^4 cells/well 24 h before the microscopy measurement. For microscopy imaging, the attached cells in IBIDI dishes were washed once with warm Hanks' balanced salt solution (HBSS, Gibco-Invitrogen); after that, 1 mL of a corresponding dye solution in warm HBSS was added and the cells were incubated for 10 min at room temperature for NR12A, NRLD, or Nile Red, 20 min at 37 °C for NRER$_F$ and NRER$_{Cl}$, and 45 min at 37 °C for NRLyso and NRMito. For the NRGolgi$_E$ probe, the attached cells in IBIDI dishes were washed twice with cold Hanks' balanced salt solution (HBSS, Gibco-Invitrogen); after that, 1 mL of a cold solution of dye conjugate with BSA (1:1 molar ratio) or with β-cyclodextrin (1:6 molar ratio) was added and the cells were incubated for 30 min at 4 °C followed by washing with warm HBSS and a further incubation for 30 min at 37 °C.

For colocalization experiments, the commercial organelle-targeting probes were added together with solvatochromic probes in the following concentrations: 50 nM of WGA Alexa 488 conjugate (Invitrogen) for NR12A; 50 nM of MitoTracker Green FM (Invitrogen) for NRMito; 50 nM of LysoTracker Green DND-26 (Invitrogen) for NRLyso; 200 (for NRER$_F$) or 500 nM (for NRER$_{Cl}$) of ERTracker Green (Invitrogen); 500 nM of BODIPY 493/503 (Invitrogen) for NRLD); 2.5 μM (in form of 1:1 molar ratio conjugate with BSA) or 150 nM (in 1 mM solution of β-cyclodextrin) of BODIPY FL C_5-ceramide (Invitrogen) for NRGolgi$_E$.

Fluorescence Microscopy. Cellular imaging was performed using a Nikon Ti-E inverted microscope, equipped with CFI Plan Apo ×60 oil (NA = 1.4) objective, X-Light spinning disk module (CREST Optics), and a Hamamatsu Orca Flash 4 sCMOS camera with a bandpass filter of 531/40 nm (Semrock) or 600/50 nm (Semrock). The excitation in confocal mode was provided by a 488 or 532 nm diode laser (OXXIUS). The exposure time in confocal mode

https://dx.doi.org/10.1021/jacs.0c10972
J. Am. Chem. Soc. XXXX, XXX, XXX−XXX

was set to 500 ms per image frame. All the images were recorded using NIS Elements and then processed using Fiji software. Pearson's correlation coefficients for colocalization were calculated using a Coloc2 Fiji plugin.

Ratiometric confocal imaging of KB cells and LUVs was performed on a Leica TSC SPE confocal microscope with HXC PL APO 63×/1.40 OIL CS objective. The excitation light was provided by a 488 nm laser, while the fluorescence was detected at two spectral ranges: 550−600 ($I_{550-600}$) and 600−650 nm ($I_{600-650}$) in sequential mode by rapid switching to minimize drift; a sum of five images is shown (20 images in case of hyperosmotic stress experiments with NR12A). All the parameters at each channel were left constant; the illumination power was adjusted to achieve a good signal for each probe. The laser power settings were as follows: 8% of max intensity for NRLD; 9% of max intensity for NRLyso; 12% of max intensity for $NRER_{Cl}$ and NRMito; 30% of max intensity for NR12A for oxidative stress experiments and 60% for hyperosmotic stress experiments; 45% of max intensity for $NRER_{F}$; 70% of max intensity for $NRGolgi_{E}$. The ratiometric images were generated by using special macros under ImageJ that divides the image of the $I_{550-600}$ channel by that of the $I_{600-650}$ channel. For each pixel, a pseudocolor scale was used for coding the ratio, while the intensity is defined by the integral intensity recorded for both channels at the corresponding pixel. Cholesterol extraction was induced by incubating the cells with 5 mM Me-β-cyclodextrin (MBCD) in reduced serum medium (Opti-MEM, Gibco Invitrogen) for 1 h at 37 °C with consecutive washing with fresh HBSS.[79] Cholesterol enrichment was induced by incubating the cells with a saturated complex of MBCD+cholesterol (48 mg/g of cholesterol) in reduced serum medium (Opti-MEM, Gibco Invitrogen) (total MBCD concentration was 5 mM) for 3 h at 37 °C followed by consecutive washing with fresh HBSS.[69] Oxidative stress was induced by incubating the cells with a 2 mM solution of H_2O_2 in HBSS for 1 h at 37 °C with consecutive washing with fresh HBSS.[80] In all cases, microscopy imaging was started 70 min after the end of incubation with H_2O_2. Hyperosmotic stress was induced by replacing half of the cell medium with a 1 M sucrose solution immediately followed by imaging.[5]

■ ASSOCIATED CONTENT

Supporting Information

The Supporting Information is available free of charge at https://pubs.acs.org/doi/10.1021/jacs.0c10972.

Figures of synthesis schemes, fluorescence emission spectra, colocalization microscopy images, imaging localization of solvatochromic organelle probes and ratiometric images and tables of absorption and fluorescence properties of probes, Pearson's correlation coefficient values, and weighted arithmetic mean values (PDF)

■ AUTHOR INFORMATION

Corresponding Author

Andrey S. Klymchenko − *Laboratoire de Bioimagerie et Pathologies, UMR 7021 CNRS, Université de Strasbourg, 67401 Illkirch, France;* orcid.org/0000-0002-2423-830X; Email: andrey.klymchenko@unistra.fr

Authors

Dmytro I. Danylchuk − *Laboratoire de Bioimagerie et Pathologies, UMR 7021 CNRS, Université de Strasbourg, 67401 Illkirch, France*

Pierre-Henri Jouard − *Laboratoire de Bioimagerie et Pathologies, UMR 7021 CNRS, Université de Strasbourg, 67401 Illkirch, France*

Complete contact information is available at: https://pubs.acs.org/10.1021/jacs.0c10972

Notes

The authors declare no competing financial interest.

■ ACKNOWLEDGMENTS

This work was supported by the European Research Council ERC Consolidator grant BrightSens 648528. D.I.D. was supported by a fellowship from the Ministère de la Recherche (France). Bohdan Wasylyk is acknowledged for providing the KB cells.

■ REFERENCES

(1) Zhu, H.; Fan, J.; Du, J.; Peng, X. Fluorescent Probes for Sensing and Imaging within Specific Cellular Organelles. *Acc. Chem. Res.* **2016**, *49*, 2115−2126.

(2) Xu, W.; Zeng, Z.; Jiang, J. H.; Chang, Y. T.; Yuan, L. Discerning the Chemistry in Individual Organelles with Small-Molecule Fluorescent Probes. *Angew. Chem., Int. Ed.* **2016**, *55*, 13658−13699.

(3) Srikun, D.; Albers, A. E.; Nam, C. I.; Iavarone, A. T.; Chang, C. J. Organelle-Targetable Fluorescent Probes for Imaging Hydrogen Peroxide in Living Cells Via Snap-Tag Protein Labeling. *J. Am. Chem. Soc.* **2010**, *132*, 4455−4465.

(4) Gao, P.; Pan, W.; Li, N.; Tang, B. Fluorescent Probes for Organelle-Targeted Bioactive Species Imaging. *Chem. Sci.* **2019**, *10*, 6035−6071.

(5) Goujon, A.; Colom, A.; Strakova, K.; Mercier, V.; Mahecic, D.; Manley, S.; Sakai, N.; Roux, A.; Matile, S. Mechanosensitive Fluorescent Probes to Image Membrane Tension in Mitochondria, Endoplasmic Reticulum, and Lysosomes. *J. Am. Chem. Soc.* **2019**, *141*, 3380−3384.

(6) Hu, F.; Liu, B. Organelle-Specific Bioprobes Based on Fluorogens with Aggregation-Induced Emission (Aie) Characteristics. *Org. Biomol. Chem.* **2016**, *14*, 9931−9944.

(7) Cerrato, C. P.; Kunnapuu, K.; Langel, U. Cell-Penetrating Peptides with Intracellular Organelle Targeting. *Expert Opin. Drug Delivery* **2017**, *14*, 245−255.

(8) Lukinavicius, G.; Reymond, L.; Umezawa, K.; Sallin, O.; D'Este, E.; Gottfert, F.; Ta, H.; Hell, S. W.; Urano, Y.; Johnsson, K. Fluorogenic Probes for Multicolor Imaging in Living Cells. *J. Am. Chem. Soc.* **2016**, *138*, 9365−9368.

(9) Lingwood, D.; Simons, K. Lipid Rafts as a Membrane-Organizing Principle. *Science* **2010**, *327*, 46−50.

(10) Sezgin, E.; Levental, I.; Mayor, S.; Eggeling, C. The Mystery of Membrane Organization: Composition, Regulation and Roles of Lipid Rafts. *Nat. Rev. Mol. Cell Biol.* **2017**, *18*, 361−374.

(11) Martin, S.; Parton, R. G. Lipid Droplets: A Unified View of a Dynamic Organelle. *Nat. Rev. Mol. Cell Biol.* **2006**, *7*, 373−378.

(12) Mesmin, B.; Maxfield, F. R. Intracellular Sterol Dynamics. *Biochim. Biophys. Acta, Mol. Cell Biol. Lipids* **2009**, *1791*, 636−645.

(13) Ikonen, E. Cellular Cholesterol Trafficking and Compartmentalization. *Nat. Rev. Mol. Cell Biol.* **2008**, *9*, 125−138.

(14) Brown, D. A.; London, E. Structure and Function of Sphingolipid- and Cholesterol-Rich Membrane Rafts. *J. Biol. Chem.* **2000**, *275*, 17221−17224.

(15) Stone, M. B.; Shelby, S. A.; Veatch, S. L. Super-Resolution Microscopy: Shedding Light on the Cellular Plasma Membrane. *Chem. Rev.* **2017**, *117*, 7457−7477.

(16) Risselada, H. J.; Marrink, S. J. The Molecular Face of Lipid Rafts in Model Membranes. *Proc. Natl. Acad. Sci. U. S. A.* **2008**, *105*, 17367−17372.

(17) Levental, K. R.; Malmberg, E.; Symons, J. L.; Fan, Y. Y.; Chapkin, R. S.; Ernst, R.; Levental, I. Lipidomic and Biophysical Homeostasis of Mammalian Membranes Counteracts Dietary Lipid Perturbations to Maintain Cellular Fitness. *Nat. Commun.* **2020**, *11*, 13.

(18) Aguilar, P. S.; de Mendoza, D. Control of Fatty Acid Desaturation: A Mechanism Conserved from Bacteria to Humans. *Mol. Microbiol.* **2006**, *62*, 1507−1514.

(19) Shyu, P.; Wong, X. F. A.; Crasta, K.; Thibault, G. Dropping in on Lipid Droplets: Insights into Cellular Stress and Cancer. *Biosci. Rep.* **2018**, *38* (5), 20180764.
(20) Vyšniauskas, A.; Kuimova, M. K. A Twisted Tale: Measuring Viscosity and Temperature of Microenvironments Using Molecular Rotors. *Int. Rev. Phys. Chem.* **2018**, *37*, 259−285.
(21) Klymchenko, A. S. Solvatochromic and Fluorogenic Dyes as Environment-Sensitive Probes: Design and Biological Applications. *Acc. Chem. Res.* **2017**, *50*, 366−375.
(22) Su, D.; Teoh, C. L.; Wang, L.; Liu, X.; Chang, Y. T. Motion-Induced Change in Emission (Mice) for Developing Fluorescent Probes. *Chem. Soc. Rev.* **2017**, *46*, 4833−4844.
(23) Haidekker, M. A.; Theodorakis, E. A. Ratiometric Mechano-sensitive Fluorescent Dyes: Design and Applications. *J. Mater. Chem. C* **2016**, *4*, 2707−2718.
(24) Dent, M. R.; Lopez-Duarte, I.; Dickson, C. J.; Geoghegan, N. D.; Cooper, J. M.; Gould, I. R.; Krams, R.; Bull, J. A.; Brooks, N. J.; Kuimova, M. K. Imaging Phase Separation in Model Lipid Membranes through the Use of Bodipy Based Molecular Rotors. *Phys. Chem. Chem. Phys.* **2015**, *17*, 18393−18402.
(25) Chambers, J. E.; Kubankova, M.; Huber, R. G.; Lopez-Duarte, I.; Avezov, E.; Bond, P. J.; Marciniak, S. J.; Kuimova, M. K. An Optical Technique for Mapping Microviscosity Dynamics in Cellular Organelles. *ACS Nano* **2018**, *12*, 4398−4407.
(26) Humeniuk, H. V.; Rosspeintner, A.; Licari, G.; Kilin, V.; Bonacina, L.; Vauthey, E.; Sakai, N.; Matile, S. White-Fluorescent Dual-Emission Mechanosensitive Membrane Probes That Function by Bending Rather Than Twisting. *Angew. Chem., Int. Ed.* **2018**, *57*, 10559−10563.
(27) Dal Molin, M.; Verolet, Q.; Colom, A.; Letrun, R.; Derivery, E.; Gonzalez-Gaitan, M.; Vauthey, E.; Roux, A.; Sakai, N.; Matile, S. Fluorescent Flippers for Mechanosensitive Membrane Probes. *J. Am. Chem. Soc.* **2015**, *137*, 568−571.
(28) Mercier, V.; Larios, J.; Molinard, G.; Goujon, A.; Matile, S.; Gruenberg, J.; Roux, A. Endosomal Membrane Tension Regulates Escrt-Iii-Dependent Intra-Lumenal Vesicle Formation. *Nat. Cell Biol.* **2020**, *22*, 947−959.
(29) Colom, A.; Derivery, E.; Soleimanpour, S.; Tomba, C.; Molin, M. D.; Sakai, N.; Gonzalez-Gaitan, M.; Matile, S.; Roux, A. A Fluorescent Membrane Tension Probe. *Nat. Chem.* **2018**, *10*, 1118−1125.
(30) Straková, K.; López-Andarias, J.; Jiménez-Rojo, N.; Chambers, J. E.; Marciniak, S. J.; Riezman, H.; Sakai, N.; Matile, S. Haloflippers: A General Tool for the Fluorescence Imaging of Precisely Localized Membrane Tension Changes in Living Cells. *ACS Cent. Sci.* **2020**, *6*, 1376−1385.
(31) Klymchenko, A. S.; Kreder, R. Fluorescent Probes for Lipid Rafts: From Model Membranes to Living Cells. *Chem. Biol.* **2014**, *21*, 97−113.
(32) Liu, C.; Tian, M.; Lin, W. A Unique Polarity-Sensitive Photothermal Sensitizer Revealing Down-Regulated Mitochondrial Polarity During Photo-Induced Cell Death. *J. Mater. Chem. B* **2020**, *8*, 752−757.
(33) Shynkar, V. V.; Klymchenko, A. S.; Kunzelmann, C.; Duportail, G.; Muller, C. D.; Demchenko, A. P.; Freyssinet, J. M.; Mely, Y. Fluorescent Biomembrane Probe for Ratiometric Detection of Apoptosis. *J. Am. Chem. Soc.* **2007**, *129*, 2187−2193.
(34) Ashoka, A. H.; Ashokkumar, P.; Kovtun, Y. P.; Klymchenko, A. S. Solvatochromic near-Infrared Probe for Polarity Mapping of Biomembranes and Lipid Droplets in Cells under Stress. *J. Phys. Chem. Lett.* **2019**, *10*, 2414−2421.
(35) Ghosh, S.; Nandi, S.; Ghosh, C.; Bhattacharyya, K. Fluorescence Dynamics in the Endoplasmic Reticulum of a Live Cell: Time-Resolved Confocal Microscopy. *ChemPhysChem* **2016**, *17*, 2818−2823.
(36) Jiang, N.; Fan, J.; Xu, F.; Peng, X.; Mu, H.; Wang, J.; Xiong, X. Ratiometric Fluorescence Imaging of Cellular Polarity: Decrease in Mitochondrial Polarity in Cancer Cells. *Angew. Chem., Int. Ed.* **2015**, *54*, 2510−2514.
(37) Amaro, M.; Reina, F.; Hof, M.; Eggeling, C.; Sezgin, E. Laurdan and Di-4-Aneppdhq Probe Different Properties of the Membrane. *J. Phys. D: Appl. Phys.* **2017**, *50*, 134004.
(38) Zhang, Y. L.; Frangos, J. A.; Chachisvilis, M. Laurdan Fluorescence Senses Mechanical Strain in the Lipid Bilayer Membrane. *Biochem. Biophys. Res. Commun.* **2006**, *347*, 838−841.
(39) Dietrich, C.; Bagatolli, L. A.; Volovyk, Z. N.; Thompson, N. L.; Levi, M.; Jacobson, K.; Gratton, E. Lipid Rafts Reconstituted in Model Membranes. *Biophys. J.* **2001**, *80*, 1417−1428.
(40) Jin, L.; Millard, A. C.; Wuskell, J. P.; Dong, X. M.; Wu, D. Q.; Clark, H. A.; Loew, L. M. Characterization and Application of a New Optical Probe for Membrane Lipid Domains. *Biophys. J.* **2006**, *90*, 2563−2575.
(41) Kwiatek, J. M.; Owen, D. M.; Abu-Siniyeh, A.; Yan, P.; Loew, L. M.; Gaus, K. Characterization of a New Series of Fluorescent Probes for Imaging Membrane Order. *PLoS One* **2013**, *8*, e52960.
(42) Oncul, S.; Klymchenko, A. S.; Kucherak, O. A.; Demchenko, A. P.; Martin, S.; Dontenwill, M.; Arntz, Y.; Didier, P.; Duportail, G.; Mely, Y. Liquid Ordered Phase in Cell Membranes Evidenced by a Hydration-Sensitive Probe: Effects of Cholesterol Depletion and Apoptosis. *Biochim. Biophys. Acta, Biomembr.* **2010**, *1798*, 1436−1443.
(43) Kucherak, O. A.; Oncul, S.; Darwich, Z.; Yushchenko, D. A.; Arntz, Y.; Didier, P.; Mely, Y.; Klymchenko, A. S. Switchable Nile Red-Based Probe for Cholesterol and Lipid Order at the Outer Leaflet of Biomembranes. *J. Am. Chem. Soc.* **2010**, *132*, 4907−4916.
(44) Castro-Castillo, V.; Gajardo, J.; Sandoval-Altamirano, C.; Gratton, E.; Sanchez, S.; Malacrida, L.; Gunther, G. Caprydaa, an Anthracene Dye Analog to Laurdan: A Comparative Study Using Cuvette and Microscopy. *J. Mater. Chem. B* **2020**, *8*, 88−99.
(45) Valanciunaite, J.; Kempf, E.; Seki, H.; Danylchuk, D. I.; Peyrieras, N.; Niko, Y.; Klymchenko, A. S. Polarity Mapping of Cells and Embryos by Improved Fluorescent Solvatochromic Pyrene Probe. *Anal. Chem.* **2020**, *92*, 6512−6520.
(46) Niko, Y.; Didier, P.; Mely, Y.; Konishi, G.; Klymchenko, A. S. Bright and Photostable Push-Pull Pyrene Dye Visualizes Lipid Order Variation between Plasma and Intracellular Membranes. *Sci. Rep.* **2016**, *6* (1), 18870.
(47) Kim, H. M.; Choo, H.-J.; Jung, S.-Y.; Ko, Y.-G.; Park, W.-H.; Jeon, S.-J.; Kim, C. H.; Joo, T.; Cho, B. R. A Two-Photon Fluorescent Probe for Lipid Raft Imaging: C-Laurdan. *ChemBioChem* **2007**, *8*, 553−559.
(48) Danylchuk, D. I.; Sezgin, E.; Chabert, P.; Klymchenko, A. S. Redesigning Solvatochromic Probe Laurdan for Imaging Lipid Order Selectively in Cell Plasma Membranes. *Anal. Chem.* **2020**, *92*, 14798−14805.
(49) Owen, D. M.; Rentero, C.; Magenau, A.; Abu-Siniyeh, A.; Gaus, K. Quantitative Imaging of Membrane Lipid Order in Cells and Organisms. *Nat. Protoc.* **2012**, *7*, 24−35.
(50) Jimenez-Sanchez, A.; Lei, E. K.; Kelley, S. O. A Multifunctional Chemical Probe for the Measurement of Local Micropolarity and Microviscosity in Mitochondria. *Angew. Chem., Int. Ed.* **2018**, *57*, 8891−8895.
(51) Iaea, D. B.; Maxfield, F. R. Membrane Order in the Plasma Membrane and Endocytic Recycling Compartment. *PLoS One* **2017**, *12*, e0188041.
(52) Li, L. L.; Li, K.; Li, M. Y.; Shi, L.; Liu, Y. H.; Zhang, H.; Pan, S. L.; Wang, N.; Zhou, Q.; Yu, X. Q. Bodipy-Based Two-Photon Fluorescent Probe for Real-Time Monitoring of Lysosomal Viscosity with Fluorescence Lifetime Imaging Microscopy. *Anal. Chem.* **2018**, *90*, 5873−5878.
(53) Guo, R.; Yin, J.; Ma, Y.; Wang, Q.; Lin, W. A Novel Mitochondria-Targeted Rhodamine Analogue for the Detection of Viscosity Changes in Living Cells, Zebra Fish and Living Mice. *J. Mater. Chem. B* **2018**, *6*, 2894−2900.
(54) Palacios-Serrato, E.; Araiza-Olivera, D.; Jiménez-Sánchez, A. Fluorescent Probe for Transmembrane Dynamics During Osmotic Effects. *Anal. Chem.* **2020**, *92*, 3888−3895.

https://dx.doi.org/10.1021/jacs.0c10972
J. Am. Chem. Soc. XXXX, XXX, XXX−XXX

(55) Greenspan, P.; Mayer, E. P.; Fowler, S. D. Nile Red - a Selective Fluorescent Stain for Intracellular Lipid Droplets. *J. Cell Biol.* **1985**, *100*, 965−973.
(56) Bongiovanni, M. N.; Godet, J.; Horrocks, M. H.; Tosatto, L.; Carr, A. R.; Wirthensohn, D. C.; Ranasinghe, R. T.; Lee, J. E.; Ponjavic, A.; Fritz, J. V.; Dobson, C. M.; Klenerman, D.; Lee, S. F. Multi-Dimensional Super-Resolution Imaging Enables Surface Hydrophobicity Mapping. *Nat. Commun.* **2016**, *7* (1), 9.
(57) Wang, H. M.; Feng, Z. Q. Q.; Del Signore, S. J.; Rodal, A. A.; Xu, B. Active Probes for Imaging Membrane Dynamics of Live Cells with High Spatial and Temporal Resolution over Extended Time Scales and Areas. *J. Am. Chem. Soc.* **2018**, *140*, 3505−3509.
(58) Danylchuk, D. I.; Moon, S.; Xu, K.; Klymchenko, A. S. Switchable Solvatochromic Probes for Live-Cell Super-Resolution Imaging of Plasma Membrane Organization. *Angew. Chem., Int. Ed.* **2019**, *58*, 14920−14924.
(59) Zielonka, J.; Joseph, J.; Sikora, A.; Hardy, M.; Ouari, O.; Vasquez-Vivar, J.; Cheng, G.; Lopez, M.; Kalyanaraman, B. Mitochondria-Targeted Triphenylphosphonium-Based Compounds: Syntheses, Mechanisms of Action, and Therapeutic and Diagnostic Applications. *Chem. Rev.* **2017**, *117*, 10043−10120.
(60) Wagner, N.; Stephan, M.; Hoglinger, D.; Nadler, A. A Click Cage: Organelle-Specific Uncaging of Lipid Messengers. *Angew. Chem., Int. Ed.* **2018**, *57*, 13339−13343.
(61) Yang, Z.; He, Y.; Lee, J. H.; Park, N.; Suh, M.; Chae, W. S.; Cao, J.; Peng, X.; Jung, H.; Kang, C.; Kim, J. S. A Self-Calibrating Bipartite Viscosity Sensor for Mitochondria. *J. Am. Chem. Soc.* **2013**, *135*, 9181−9185.
(62) Kong, X.; Yin, J.; Li, M.; Zhu, L.; Dong, B.; Ma, Y.; Lin, W. Simultaneously Imaging of So2 in Lysosomes and Mitochondria Based on a Dual Organelle-Targeted Fluorescent Probe. *Sens. Actuators, B* **2019**, *292*, 80−87.
(63) Zhang, H.; Fan, J.; Dong, H.; Zhang, S.; Xu, W.; Wang, J.; Gao, P.; Peng, X. Fluorene-Derived Two-Photon Fluorescent Probes for Specific and Simultaneous Bioimaging of Endoplasmic Reticulum and Lysosomes: Group-Effect and Localization. *J. Mater. Chem. B* **2013**, *1*, 5450−5455.
(64) Hirayama, T.; Inden, M.; Tsuboi, H.; Niwa, M.; Uchida, Y.; Naka, Y.; Hozumi, I.; Nagasawa, H. A Golgi-Targeting Fluorescent Probe for Labile Fe(Ii) to Reveal an Abnormal Cellular Iron Distribution Induced by Dysfunction of Vps35. *Chem. Sci.* **2019**, *10*, 1514−1521.
(65) Collot, M.; Fam, T. K.; Ashokkumar, P.; Faklaris, O.; Galli, T.; Danglot, L.; Klymchenko, A. S. Ultrabright and Fluorogenic Probes for Multicolor Imaging and Tracking of Lipid Droplets in Cells and Tissues. *J. Am. Chem. Soc.* **2018**, *140*, 5401−5411.
(66) Steinkuhler, J.; Sezgin, E.; Urbancic, I.; Eggeling, C.; Dimova, R. Mechanical Properties of Plasma Membrane Vesicles Correlate with Lipid Order, Viscosity and Cell Density. *Commun. Biol.* **2019**, *2* (1), 337.
(67) Tabas, I. Consequences of Cellular Cholesterol Accumulation: Basic Concepts and Physiological Implications. *J. Clin. Invest.* **2002**, *110*, 905−911.
(68) Carstea, E. D.; Morris, J. A.; Coleman, K. G.; Loftus, S. K.; Zhang, D.; Cummings, C.; Gu, J.; Rosenfeld, M. A.; Pavan, W. J.; Krizman, D. B.; Nagle, J.; Polymeropoulos, M. H.; Sturley, S. L.; Ioannou, Y. A.; Higgins, M. E.; Comly, M.; Cooney, A.; Brown, A.; Kaneski, C. R.; BlanchetteMackie, E. J.; Dwyer, N. K.; Neufeld, E. B.; Chang, T. Y.; Liscum, L.; Strauss, J. F.; Ohno, K.; Zeigler, M.; Carmi, R.; Sokol, J.; Markie, D.; Oneill, R. R.; vanDiggelen, O. P.; Elleder, M.; Patterson, M. C.; Brady, R. O.; Vanier, M. T.; Pentchev, P. G.; Tagle, D. A. Niemann-Pick C1 Disease Gene: Homology to Mediators of Cholesterol Homeostasis. *Science* **1997**, *277*, 228−231.
(69) Zidovetzki, R.; Levitan, I. Use of Cyclodextrins to Manipulate Plasma Membrane Cholesterol Content: Evidence, Misconceptions and Control Strategies. *Biochim. Biophys. Acta, Biomembr.* **2007**, *1768*, 1311−1324.
(70) Yin, H.; Xu, L.; Porter, N. A. Free Radical Lipid Peroxidation: Mechanisms and Analysis. *Chem. Rev.* **2011**, *111*, 5944−5972.
(71) Nilsson, E.; Ghassemifar, R.; Brunk, U. T. Lysosomal Heterogeneity between and within Cells with Respect to Resistance against Oxidative Stress. *Histochem. J.* **1997**, *29*, 857−865.
(72) Lenaz, G. Role of Mitochondria in Oxidative Stress and Ageing. *Biochim. Biophys. Acta, Bioenerg.* **1998**, *1366*, 53−67.
(73) Ott, M.; Gogvadze, V.; Orrenius, S.; Zhivotovsky, B. Mitochondria, Oxidative Stress and Cell Death. *Apoptosis* **2007**, *12*, 913−922.
(74) Mammoto, T.; Mammoto, A.; Ingber, D. E. Mechanobiology and Developmental Control. *Annu. Rev. Cell Dev. Biol.* **2013**, *29*, 27−61.
(75) Ladoux, B.; Mege, R. M. Mechanobiology of Collective Cell Behaviours. *Nat. Rev. Mol. Cell Biol.* **2017**, *18*, 743−757.
(76) Chaudhuri, P. K.; Low, B. C.; Lim, C. T. Mechanobiology of Tumor Growth. *Chem. Rev.* **2018**, *118*, 6499−6515.
(77) Alam Shibly, S. U.; Ghatak, C.; Sayem Karal, M. A.; Moniruzzaman, M.; Yamazaki, M. Experimental Estimation of Membrane Tension Induced by Osmotic Pressure. *Biophys. J.* **2016**, *111*, 2190−2201.
(78) Deda, M. L.; Ghedini, M.; Aiello, I.; Pugliese, T.; Barigelletti, F.; Accorsi, G. Organometallic Emitting Dyes: Palladium(Ii) Nile Red Complexes. *J. Organomet. Chem.* **2005**, *690*, 857−861.
(79) Onodera, R.; Motoyama, K.; Okamatsu, A.; Higashi, T.; Kariya, R.; Okada, S.; Arima, H. Involvement of Cholesterol Depletion from Lipid Rafts in Apoptosis Induced by Methyl-B-Cyclodextrin. *Int. J. Pharm.* **2013**, *452*, 116−123.
(80) de la Haba, C.; Palacio, J. R.; Martinez, P.; Morros, A. Effect of Oxidative Stress on Plasma Membrane Fluidity of Thp-1 Induced Macrophages. *Biochim. Biophys. Acta, Biomembr.* **2013**, *1828*, 357−364.

https://dx.doi.org/10.1021/jacs.0c10972
J. Am. Chem. Soc. XXXX, XXX, XXX−XXX